Origin of bedding-parallel calcite "beef" layers in the Upper Jurassic Haynesville shale, northwestern Louisiana

L. Taras Bryndzia, Calum I. Macaulay, Alexander P. Litvinchuk, and Brian D. Monteleone

ABSTRACT

Bedding-parallel calcite layers (BPCLs) preserving a fibrous "beef" texture are common throughout the overmature Haynesville Formation shale. Their interfaces with the host shale contain radiating splays of anhydrite pseudomorphs after gypsum rosettes, suggesting either a primary evaporitic or an early burial origin. In places, the calcite layers contain remnant barite or anhydrite in crystallographic alignment with its host calcite, indicating that the calcite formed by replacing a fibrous sulfate precursor phase.

During burial and heating, maturation of source rock organic matter resulted in the expulsion of hydrocarbons (oil and gas). Consequently, the redox state of the shale and hydrocarbon system became reducing, as indicated by the ubiquitous presence of H₂S. Both anhydrite and barite are unstable in the presence of H₂S and were consumed by thermochemical sulfate reduction. At peak burial, liquid hydrocarbons cracked to CH₄ gas and remnant solid pyrobitumen, which typically occupies the median suture zone of the fibrous calcite layers. It was along this median suture that calcite replacement of anhydrite and barite was initiated, proceeding to replace sulfate minerals from the center of the layer out toward the shale contact.

We estimated the in situ CH₄ pressure attending thermochemical sulfate reduction in the Haynesville shale by using microlaser Raman spectroscopy to directly measure the density of CH₄ gas inclusions in BPCLs. Average fluid pressure gradients preserved within the fibrous calcite are approximately 0.87 ± 0.03 psi/ft ($\pm 1\sigma$; n=4), considerably above hydrostatic but below both overburden and shale fracture gradients. We found

Copyright ©2024. The American Association of Petroleum Geologists. All rights reserved.

Manuscript received October 29, 2021; provisional acceptance February 23, 2022; revised manuscript received March 29, 2022; revised manuscript provisional acceptance June 9, 2022; 2nd revised manuscript received July 26, 2022; 2nd revised manuscript provisional acceptance November 30, 2022; 3rd revised manuscript received January 4, 2023; final acceptance January 19, 2023; preliminary ahead of print version published May 15, 2023.

DOI:10.1306/01192321189

AUTHORS

L. Taras Bryndzia ~ Shell International Exploration and Production Inc., Houston, Texas; present address: independent geoscientist, Houston, Texas; ltbryndzia@gmail.com

L. Taras Bryndzia was a principal research geochemist, subject matter expert for inorganic geochemistry, and senior principal science expert for earth sciences at Shell International Exploration and Production. His research interests include stable isotope and brine geochemistry, diagenetic processes, and prediction of H₂S and Hg solubility in hydrocarbons. He holds degrees in geology from La Trobe University (B.Sc. Honors degree), and ore deposits geology (M.Sc. degree) and geochemistry (Ph.D.) from the University of Toronto.

CALUM I. MACAULAY ~ Shell Exploration and Production Company, Houston, Texas; calum.macaulay@shell.com

Calum I. Macaulay is a senior sedimentary petrologist at Shell Exploration and Production Company. He has a Ph.D. in clastic diagenesis from the University of Strathclyde and a B.Sc. (Honors) degree in geology and mineralogy from the University of Aberdeen, both located in Scotland. He joined Shell in 2001 and is currently the subject matter expert for clastic sedimentary petrology and reservoir quality.

ALEXANDER P. LITVINCHUK ~ Department of Physics, Texas Center for Superconductivity, University of Houston, Houston, Texas; litvin@central.uh.edu

Alexander P. Litvinchuk is a principal investigator and manager of the Raman and Infrared Research Laboratory at the Texas Center for Superconductivity, University of Houston, Houston, Texas. His main research area is the study of the optical properties of matter. He graduated from the Taras Shevchenko National University of Kyiv (Ukraine) and holds a Ph.D. and a D.Sc. from the Ukrainian Academy of Sciences.

BRIAN D. MONTELEONE ~ Woods Hole Oceanographic Institution, Woods Hole, Massachusetts; bmonteleone@whoi.edu Brian D. Monteleone is the laboratory manager of the Northeast National Ion Microprobe Facility at the Woods Hole Oceanographic Institution. He specializes in the development of secondary ion mass spectrometry analytical techniques for research in isotope geochemistry, volcanology, and geochronology. He holds a B.A. degree in geology and mathematics (College of Wooster) and graduate degrees in geoscience (M.Sc. degree, University of Arizona; Ph.D., Syracuse University).

ACKNOWLEDGMENTS

We thank Shell management for permission to publish the results of this study. Discussions on H₂S in the Haynesville shale with many Shell colleagues are also gratefully acknowledged, particularly those with Matt Hackworth, Anthony Salem, Paul Smith, Alan S. Kornacki, and Nathan Wilkens.

We thank J.-P. Nicot and Ursula Hammes from the Bureau of Economic Geology (The University of Texas at Austin) for sharing data from their laboratory studies on the NFR Energy Huffman 1 well, part of the Shell University of Texas Unconventional Resources project, and for help in sampling cores from the Werner anhydrite in the Shell Crocker 1 well, respectively. We also thank Ryan Williams of TerraTek, who performed the sulfate leachate extractions on crushed samples of Havnesville core material. We gratefully acknowledge Nobumichi Shimizu and Peter Landry of Woods Hole Oceanographic Institution for support with the secondary ion mass spectrometry analyses, Steven M. Bates of the Lyons Biogeochemistry Laboratory (University of California, Riverside) for help with bulk sulfur isotope analyses, and Steven C. Bergman for providing the Potosi barite sample used as a sulfur isotope standard for this study.

We owe a huge debt of gratitude to our former Shell colleague Stanley Milam for his assistance in designing the apparatus that was deployed in the field for sampling H₂S separator gas and for designing the capillary pressure system and CaF₂ optical cell used to calibrate the zero-pressure intercept for our microlaser Raman spectrometer.

no evidence to suggest that fluid pressures exceeded lithostatic or that fibrous calcite grew in dilated vein systems from their margins toward the center of the BPCLs.

The replacement of primary bedded anhydrite and barite by calcite preserves the original orientation of the precursor sulfate minerals—in other words, their fibrous beef texture is an inherited feature. The replacement of sulfate by calcite results in a solid volume loss of approximately 20 to 30 vol. %. Collapse of the layers due to loss of volume and overburden stress results in the minimum horizontal stress being parallel to bedding. Pyrobitumen layers were compressed and disaggregated due to tensile failure. Both late-stage calcite and disaggregated pyrobitumen subsequently grew in the direction of minimum horizontal stress (i.e., parallel to bedding).

INTRODUCTION

Bedding-parallel calcite layers (BPCLs), characterized by a unique mineral texture reminiscent of beef filet and commonly referred to as calcite "beef" or calcite "beef veins," are a common feature in ancient sedimentary basins containing organic-rich marine source rock shales. Fibrous calcite is generally oriented orthogonal to bedding in the host shales.

Vertical development of calcite fibers has been attributed by many researchers as indicative of syntaxial growth, implying that its primary growth was toward the center of the layer that was open, presumably due to high in situ fluid pressures during vein formation (e.g., Machel, 1985; Zanella et al., 2015; Abaab et al., 2021). It has also been suggested that under certain conditions it may be plausible for calcite growth to occur due to a balance between fluid overpressures and force of crystallization maintaining veins open during crystal growth (Wiltschko and Morse, 2001; Hilgers and Urai, 2005). Alternatively, others have concluded that such fibrous growth of calcite indicates antitaxial growth, outward from the center of the layer toward the wall rock (e.g., van der Pluijm and Marshak, 2004; Rodrigues et al., 2009; Cobbold et al., 2013). In both scenarios, a median suture appears toward the center of the calcite layer.

The global distribution of BPCLs and their mineralogical, textural, structural, and geomechanical features were thoroughly documented in a review paper by Cobbold et al. (2013). Of the 110 locations in which they documented calcite beef, Cobbold et al. (2013) reported only 29 localities containing gypsum beef. The most common host rocks for gypsum beef are mudstones or evaporites, and the most common ages are either Middle Triassic or Neogene. By contrast, they report few occurrences of gypsum beef in lower Paleozoic or Jurassic–Cretaceous host rocks. In areas of low thermal maturity, such as in many of the Jurassic (Kimmeridgian) exposures of immature organic-rich mudrocks in the United

Kingdom, calcite beef containing fibrous minerals in BPCLs is often described as consisting of fibrous calcite spar or satin spar (i.e., gypsum). Calcite beef has also been variously described as consisting of "layers of fibrous carbonate of lime and of fibrous sulfate of lime" (Cobbold et al., 2013, and references therein). Relative to celestite and gypsum, the occurrence of barite is rarely mentioned.

The focus of this contribution is BPCLs from the organic-rich Upper Jurassic Haynesville Formation (Haynesville shale) and the Bossier Formation (Bossier shale) in northwestern Louisiana in the United States. This area is a prolific shale gas producer and is an age-equivalent analog to the Kimmeridgian and Vaca Muerta Formation shales in the United Kingdom and the Neuquén Basin, Argentina, respectively. Much speculation still exists around the origin of BPCLs and the assumed fluid pressure regime under which they formed, with most hypotheses invoking a structural and/or tectonic component in their formation; hence, they are referred to as BPC veins. We recognize two distinct types of BPCLs in the Haynesville shale. The dominant type contains calcite layers with fibrous beef texture (i.e., BPCLs), often with evidence of replacement by calcite of a precursor sulfate mineral either barite or anhydrite. The other type of BPCL shows evidence of a late-stage diagenetic overprint due to hydrothermal alteration by a high-temperature, high-salinity evaporite-derived brine.

Here, we present carbon, oxygen, and sulfur isotopic data for calcite- and sulfur-bearing phases from beef-textured BPCLs. We integrate fluid inclusion (FI) data with directly measured densities of CH_4 in gas-bearing inclusions using microlaser Raman spectroscopy to infer the pressure and temperature conditions of formation of the calcite beef layers. Together with an equation of state model, the pressure-volume-temperature properties of CH_4 , CO_2 , and water mixtures were used to infer the fluid pressure gradients present at the time of calcite beef formation. Combining oxygen isotope data from gypsum in the Neuquén Basin with FI thermometry on calcite in BPCLs, together with an equilibrium oxygen isotope model for water in equilibrium with gypsum, we show that the likely source of water from which calcite in BPCLs formed was derived from the dehydration of the original gypsum layers.

Results from our study suggest that BPCLs are secondary diagenetic features that formed due to the replacement by calcite of the primary sedimentary sulfate minerals gypsum and barite. The primary sulfate minerals were most likely evaporitic and appear to have been deposited coevally with their organic-rich host mudrocks.

HAYNESVILLE SHALE

The Haynesville shale is an organic- and carbonate-rich clastic mudstone unit interpreted to have been deposited in a partly This paper benefited from reviews by former Shell colleagues Timothy N. Diggs and Ruarri J. Day-Stirrat and numerous *AAPG Bulletin* reviewers. We gratefully acknowledge the guidance provided by Kitty Milliken, Ursula Hammes, and *AAPG Bulletin* associate editor Julia F. W. Gale.

DATASHARE 179

Supplementary data and methods are available in an electronic version on the AAPG website (www.aapg.org/datashare) as Datashare 179.

euxinic and anoxic basin during the Kimmeridgian to early Tithonian, coeval with a global marine transgression that deposited organic-rich black shales in many parts of the world (Hammes et al., 2011). Figure 1 shows the location of Haynesville shale wells discussed in this paper. Details on the sedimentology and stratigraphy of the Haynesville-Bossier shales have been discussed previously by Hammes et al. (2011) and Hammes and Frébourg (2012). The Haynesville shale contains almost equal volumes of quartz and clay minerals with variable carbonate content (Figure 2; Bryndzia and Braunsdorf, 2014). It is an overmature, marine type II source rock with equivalent vitronite reflectance (VR_e) values of approximately 2% to 3%. It is a world-class gas shale resource, producing predominantly dry CH₄ and CO₂ (94:6 molar; Bryndzia et al., 2017).

Organic matter in the Haynesville shale matrix is dominated by bitumen and pyrobitumen. Two generations of bituminous material are observed. One type, prevalent throughout the shale matrix, is anisotropic and displays specular bird's-eye extinction and has a moderate VR_e of approximately 1.4% to 1.7%. The other is a pyrobitumen phase that is isotropic in reflected light, with a VRe of 2.3% to 3% and occurs as a pore-lining phase and as spheres in the shale matrix. It dominates the median sutures of BPCLs and is interpreted to be a late phase formed during oil-to-gas cracking of liquid oil at peak burial (Novosel et al., 2010). The present-day conditions in the Haynesville shale are approximately 160°C and approximately 70 MPa (Bryndzia et al., 2017). Gas production in the Havnesville shale also has associated low background levels of H₂S, generally less than 100 ppm (Bryndzia et al., 2017; Bryndzia and Macaulay, 2018).

Shale Mineralogy and Total Organic Carbon

The Haynesville and overlying prodelta Bossier shales have very different bulk mineralogical compositions. The Bossier shale is more uniform in composition and contains much less carbonate material than does the Haynesville shale (Figure 2). The Haynesville and basal Bossier source rocks contain approximately 1.5–5.0 wt. % total organic carbon (*TOC*). The upper Bossier and lower Bossier are generally much leaner (<1.5 wt. % *TOC*). It is difficult to determine with

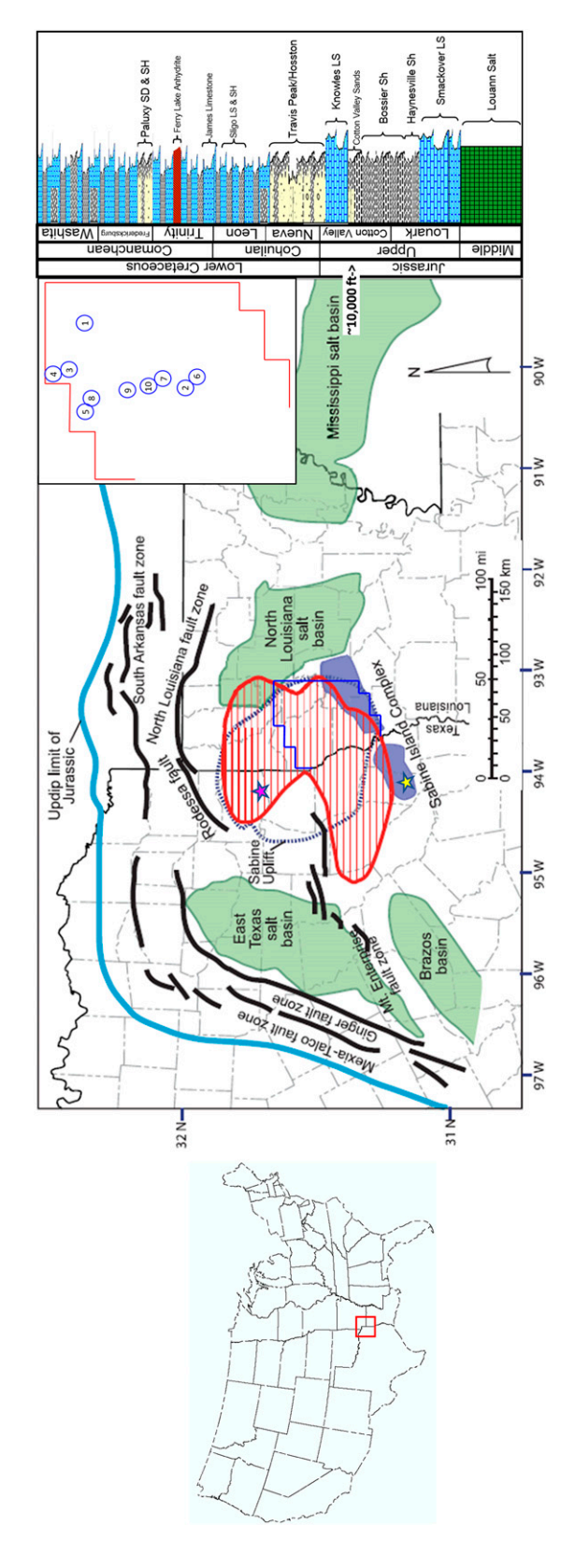
confidence what kind of kerogen Haynesville shale originally contained due to its high level of thermal maturity. Novosel et al. (2010) estimated the restored average richness of the Haynesville source-rock interval ranged from approximately 3 to 7 wt. % TOC across the study area shown in Figure 1.

Mineralogy and Textures of BPCLs in the Haynesville Shale

The BPCLs in the Haynesville shale bear a strong resemblance to those described previously for the Vaca Muerta Formation by Rodrigues et al. (2009), Cobbold et al. (2013), Gale et al. (2014), Eberli et al. (2017), Lejay et al. (2017), Małachowska et al. (2017), Ukar et al. (2017), and Weger et al. (2019). The BPCLs in Figures 3 to 6 are from different wells in the Haynesville-Bossier shale and illustrate many common features that are typical of BPCLs. Some are massive and contain only calcite, whereas others have an obvious median suture containing variable amounts of solid pyrobitumen and pyrite ± barite ± anhydrite.

Almost every BPCL that we have examined in the Haynesville shale shows evidence that the primary minerals in these layers were syngenetic layers of barite and/or gypsum (Figures 4–7). The replacement by calcite is postulated to have happened later in the burial history of the shale. Evidence for this timing is that the replacement of original sulfate minerals appears to be closely associated with the expulsion and migration of liquid oil from the organic-rich source rock.

Original gypsum rosettes, now pseudomorphed by anhydrite (Figure 4C), and barite precipitation are unlikely to have formed in a dilating vein system during burial. Gypsum rosettes typically are indicators of arid and evaporitic near-surface conditions, as is coevally precipitated barite (Cody and Cody, 1988). We propose that the fibrous BPCLs are diagenetic replacement features of original syngenetic, sulfate-rich evaporitic horizons that formed during or shortly after deposition of the organic-rich shales. Eustice and Land (1994) demonstrated that in southwestern Alabama, the basal Buckner Member of the Haynesville Formation comprises a thick unit of anhydrite after gypsum. Mancini et al. (1990) describe numerous occurrences of anhydritic shales and thin anhydrite beds within the Havnesville shale



outline). An idealized stratigraphic column for the Haynesville Formation and Bossier Formation shales is shown at right. Wells discussed in this paper lie within the area outlined in dark blue (numbered in inset at upper right). Green areas are basins and shaded blue areas are structural highs. Yellow and pink stars show the locations of the Shell Crocker 1 and NFR Energy Huffman 1 wells, respectively. The dark blue stippled outline is the extent of the Sabine uplift (modified after Hammes et al., 2011). LS = limestone; SD = sand; Figure 1. Map of eastern Texas and western Louisiana (red box in index figure), showing Late Jurassic structural elements and the Haynesville Formation shale productive area (red SH = shale.

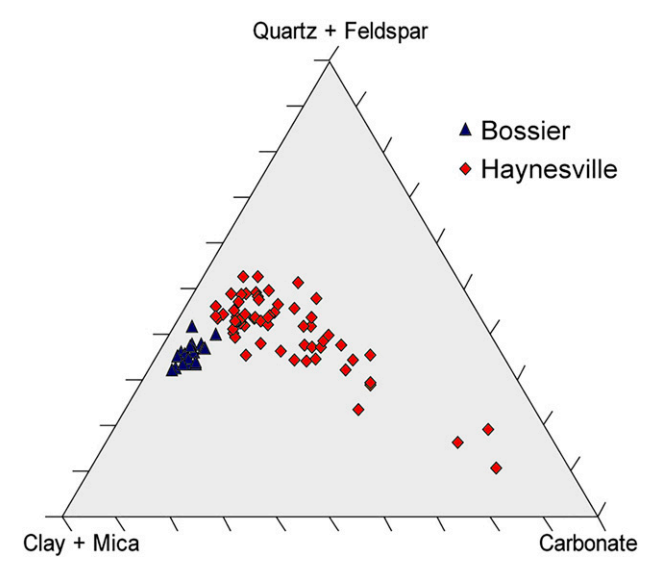


Figure 2. Ternary plot showing the range of mineralogical compositions, as determined by x-ray diffraction, in shale source rocks from the Upper Jurassic Haynesville Formation and Bossier Formation shales (modified after Bryndzia and Braunsdorf, 2014).

of the Mississippi Interior Salt Basin of Alabama, and the wider region contains three significant anhydrite units—the Werner anhydrite, the Pine Hill Anhydrite Member in the upper Louann Salt, and the Buckner Formation anhydrite—which together indicate regional extensive evaporative shallow water conditions through the Middle and Late Jurassic.

Hydrothermal Alteration of BPCLs in the Haynesville Shale

Figure 8 shows a disaggregated pyrobitumen layer along the median of a BPCL and shows the almost symmetrical distribution of an alteration selvage that formed between the host shale and median zone of the calcite layer. The alteration selvage consists of an assemblage of euhedral crystals of pure albite, quartz, and sphalerite (ZnS). The albite crystals are commonly associated with chlorite (Figure 8).

Figure 9 shows a BPCL from well 4. The image shows concave deformation of the layer boundaries into the BPCL, with subsequent brittle deformation of the median pyrobitumen layer. The remnants of the original calcite beef are preserved as rectangular islands containing central cores of disaggregated pyrobitumen, isolated within later white calcite that lacks pyrobitumen. Late-stage calcite vertical pillar growth has generated what appears to be a dominant calcite

fabric with crystal growth oriented parallel to bedding (i.e., orthogonal to the original orientation of calcite beef).

DATA AND METHODS

Details of analytical methods, data analysis, and results are provided in the supplementary data and methods (supplementary material available as AAPG Datashare 179 at www.aapg.org/datashare).

Carbon and oxygen isotopes were measured on 15 samples of calcite—9 from BPCLs, and 6 from vertical calcite veins. The samples were analyzed by Isolabs, a commercial stable isotope vendor. Oxygen isotopic compositions of water recovered from crystalline gypsum in the Neuquén Basin were taken from published data by Lo Forte et al. (2005).

Sulfur isotopes were measured on samples of H₂S gas collected at various separators in the field, precipitated as acanthite (Ag₂S). Bulk sulfur isotopes were also measured on pyrite and solid hydrocarbons (SHC) sampled from various Haynesville cores and on Werner anhydrite sampled in cores from the Shell Crocker 1 well. Sulfur isotopic data were measured at the Lyons Biogeochemistry Laboratory (University of California, Riverside) and by Isolabs. In addition, three samples of Werner anhydrite were analyzed by Coastal Science Laboratories in Austin, Texas. Seven samples of Haynesville core were crushed and soluble sulfate extracted using deionized (DI) water at Terra-Tek Laboratories (now SLB) in Salt Lake City, Utah. The sulfate was precipitated as BaSO₄ by mixing with a BaCl₂ solution. The precipitated barite was analyzed at the Lyons Biogeochemistry Laboratory.

Sulfur isotopic compositions from sulfur-bearing minerals at the thin section scale were analyzed at Woods Hole Oceanographic Institution (WHOI) using secondary ion mass spectrometry (SIMS). We established some of our own SIMS sulfur mineral standards based on multiple analyses of high-grade mineral separates that were previously analyzed at the Lyons Biogeochemistry Laboratory, as well as using standards supplied by WHOI (Appendix A.1.2 [supplementary material available as AAPG Datashare 179 at www.aapg.org/datashare]).

The FI homogenization temperatures were measured by Fluid Inclusion Technologies (now SLB) on doubly polished thin section wafers sampled from

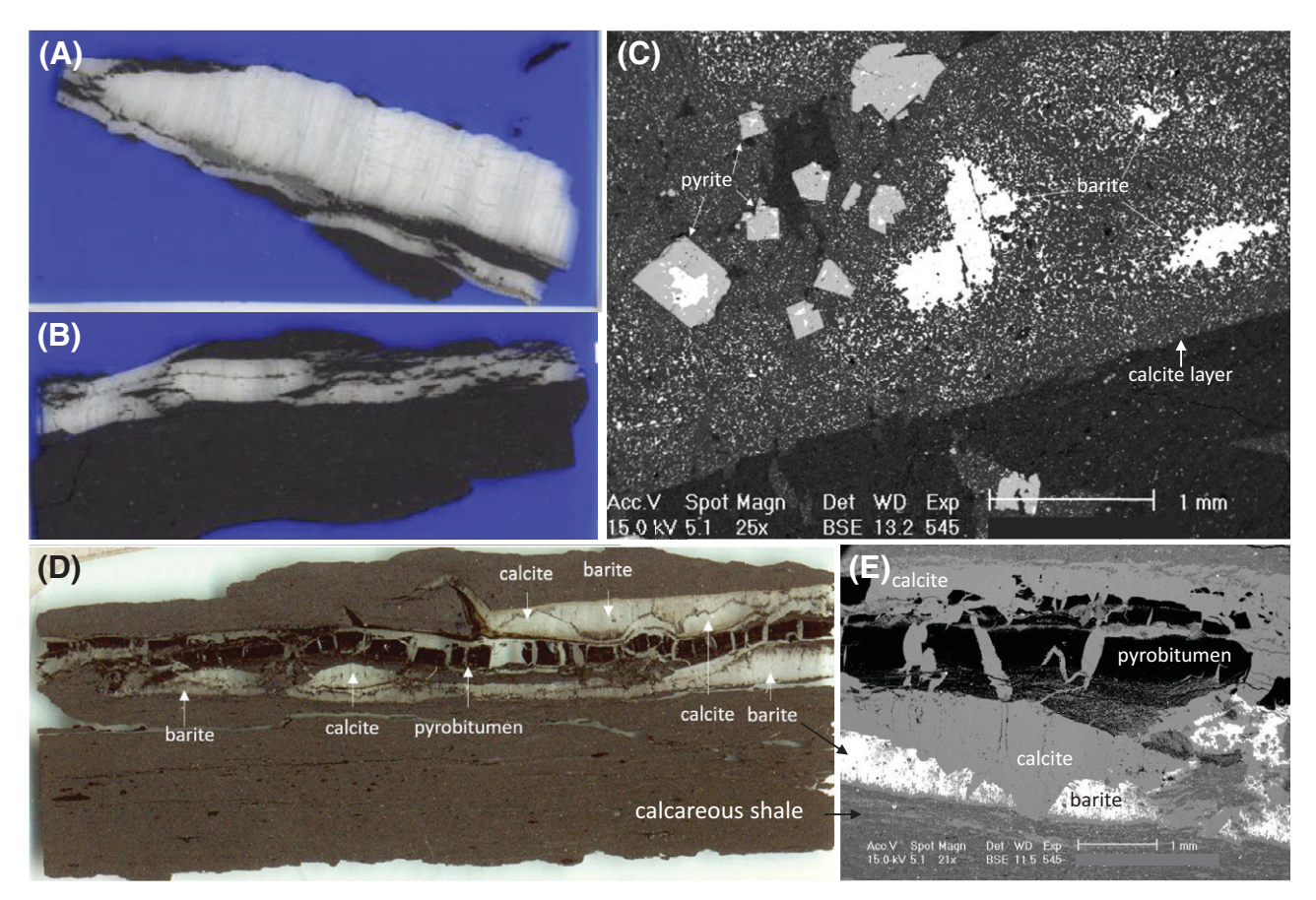


Figure 3. (A) Bedding-parallel calcite layers (BPCLs) showing fibrous calcite texture oriented perpendicular to bedding. (B) The BPCLs with a well-defined central suture containing finely dispersed pyrobitumen. (C) Primary bedded barite layer replaced by calcite (dark matrix) with coarse, recrystallized pyrite grains containing cores of relict barite. The arrow at calcite layer shows the boundary between the calcite layer and host shale. (D) Calcite replacing primary bedded barite layer with a disaggregated median layer of pyrobitumen. Note the undulatory replacement boundary within the layer showing replacement of primary barite from the center outward toward the boundary with the host shale. (E) Scanning electron microscopy image showing calcite replacement of barite layer in (D). Thin-section images (A), (B), and (D) are all 3 in. (7.6 cm) in length. AccV. = accelerating voltage; BSE = backscattered electron; Det = detector; Exp = exposure; Magn = magnification.

BPCLs in 10 Haynesville and Bossier cores. The same FI wafers were then used for microlaser Raman spectroscopy to measure the density of CH_4 gas inclusions.

RESULTS

Carbon, Oxygen, and Sulfur Isotopes

The δ^{13} C values ranged from +2‰ to +5‰ (Vienna Peedee belemnite [VPDB]) in BPCLs, and +4‰ to +6.5‰ (VPDB) in the later vertical calcite vein set. The δ^{18} O values ranged from -11‰ to -9‰ (VPDB), with similar isotopic compositions obtained for both sets of samples (Figure 10; Table A1.1

[supplementary material available as AAPG Datashare 179 at www.aapg.org/datashare]).

Bulk sulfur isotopic compositions of pyrite, SHC, and anhydrite from BPCLs are summarized in Table A1.2 (supplementary material available as AAPG Datashare 179 at www.aapg.org/datashare). Samples of the Werner anhydrite are from the Shell Crocker 1 well, located approximately 90 km south-southwest of the Haynesville gas shale in northeastern Texas (Figure 1). This is the closest penetration of the Werner anhydrite to our study area, and the core is accessible through the core repository located at the Bureau of Economic Geology (BEG) at The University of Texas at Austin. Table A1.3 (supplementary material available as AAPG Datashare 179 at www.aapg.org/datashare) contains the sulfur isotopic

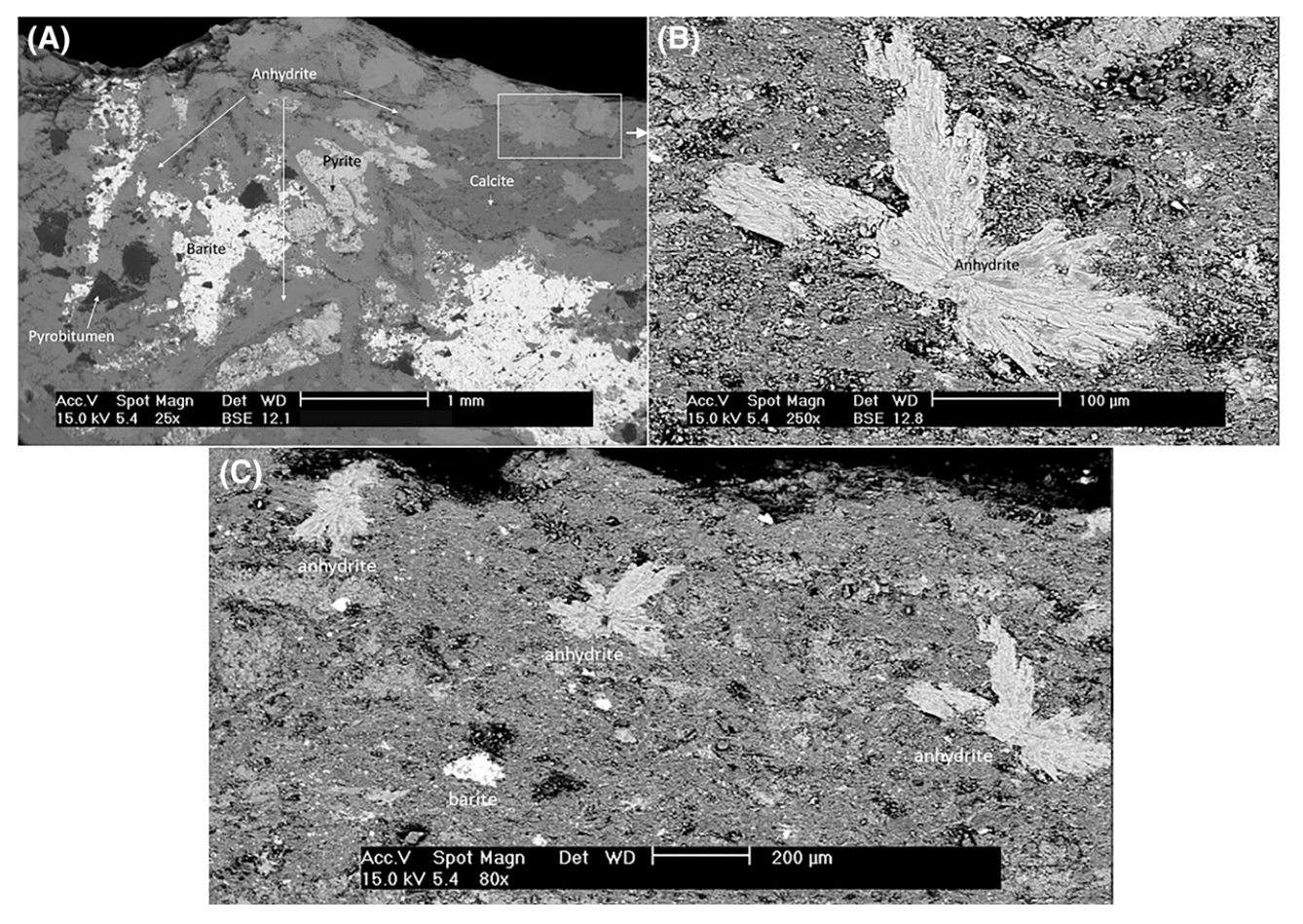


Figure 4. Scanning electron microscopy images showing the interface of a bedding-parallel calcite layer and host shale in well 5. (A–C) Remnant barite and numerous rosettes of anhydrite pseudomorphs after primary gypsum at various stages of replacement by calcite. The dark gray matrix in (B) and (C) is calcite, as noted in (A). Note the different scales in (A)–(C). Acc.V = accelerating voltage; BSE = back-scattered electron; Det = detector; Magn = magnification; WD = working distance.

composition of H_2S sampled in gas wells throughout the Haynesville shale as well as matrix sulfate leached out of crushed samples of Haynesville shale.

Matrix pyrite in the Haynesville shale is dominantly framboidal pyrite, and it has a sulfur isotopic composition that clusters in a relatively tight range, from approximately -9% to -20% (Figure 11A, B). Figure 11C, D plots the results of SIMS $\delta^{34}S$ in sulfate minerals from the various Haynesville shale wells. Figure 11E is a plot of $\delta^{34}S$ in H_2S sampled in the Haynesville shale, and falls into two distinct groups.

One group has negative sulfur isotopic compositions, with $\delta^{34}S$ ranging from -13.7% to -20.7%, whereas the other group has positive $\delta^{34}S$ values ranging from +12.4% to +18.7%. The first group has a sulfur isotopic composition that closely matches that of the coexisting framboidal matrix pyrite (-20% to -9%), whereas the other group overlaps

the range of sulfur isotopic values that are characteristic of the underlying Jurassic Werner anhydrite (+15.3‰ to +20.2‰), shown in Figure 11C, D. The δ^{34} S in H₂S from the overlying Bossier shale is indistinguishable from that in the matrix framboidal pyrite (Figure 11E). Figure 11D shows the δ^{34} S of sulfate that was leached from the shale matrix using DI water and precipitated as BaSO₄. The leachate sulfur isotopic compositions fall intermediate to end member compositions defined by matrix framboidal pyrite and the underlying Werner anhydrite (Figure 11D).

The only source of the isotopically light and negative sulfur in our data set is the sulfur associated with shale matrix SHC and framboidal pyrite. To determine if marine sulfate-bearing layers were contributing to the isotopically light H_2S , we undertook a detailed ion microprobe study of sulfur isotopes in sulfate and pyrite from the BPCLs sampled in 10 wells that

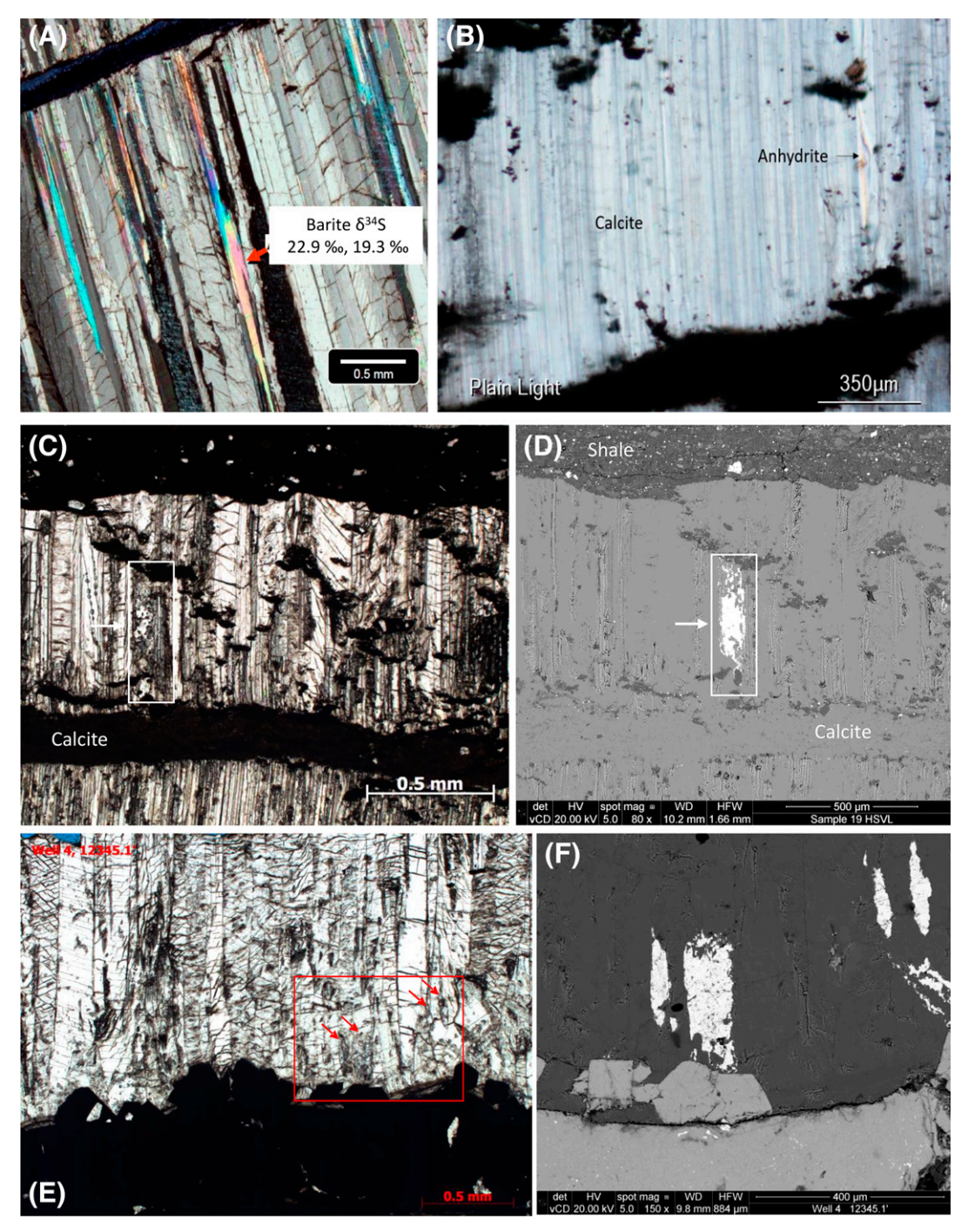
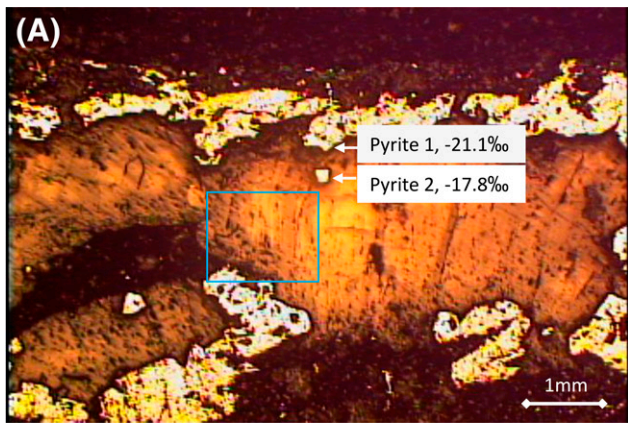
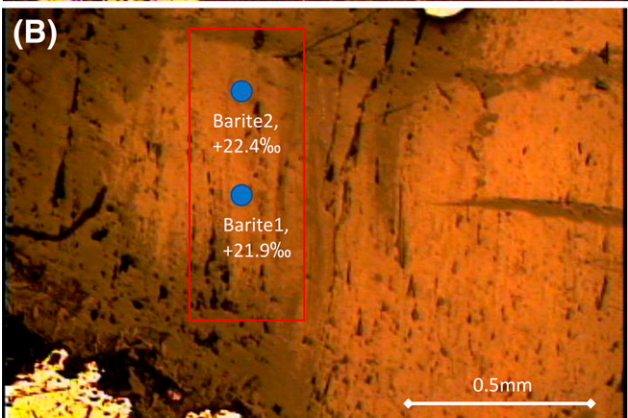


Figure 5. Images of fibrous calcite from fluid inclusion wafers of bedding-parallel calcite layers (BPCLs) in Haynesville Formation shale. The polarized light image in (A) shows relict barite after replacement by fibrous calcite—well 5. (B) Similar texture to (A), but fibrous calcite has replaced preexisting anhydrite—well 3. (C) Transmitted light image of relict barite (white rectangle) replaced by fibrous calcite in BPCLs—well 3. (D) Backscattered electron (BSE) image of same area as in (C), showing relict barite replaced by fibrous calcite in BPCLs. Note that the fibrous calcite texture is difficult to discern in BSE images. (E) Transmitted light image of relict barite replaced by fibrous calcite in BPCLs from well 4. Arrows show relict barite grains aligned parallel to fibrous calcite. (F) A BSE image of red square in (E), showing relict barite aligned parallel to calcite fibers. The δ^{34} S of barite in well 4 ranged from 17.6‰ to 25‰ (see Table A1.5 [supplementary material available as AAPG Datashare 179 at www.aapg.org/datashare]). Mineral compositions were confirmed by scanning electron microscopy and energy-dispersive analysis by x-ray. Birefringence colors are high due to the thickness of the fluid inclusion wafers used for secondary ion mass spectrometry analysis. det = detector; HFW = horizontal field width; HSVL = Haynesville; HV = high voltage; mag = magnification; vCD = low-voltage high-contrast detector; WD = working distance.





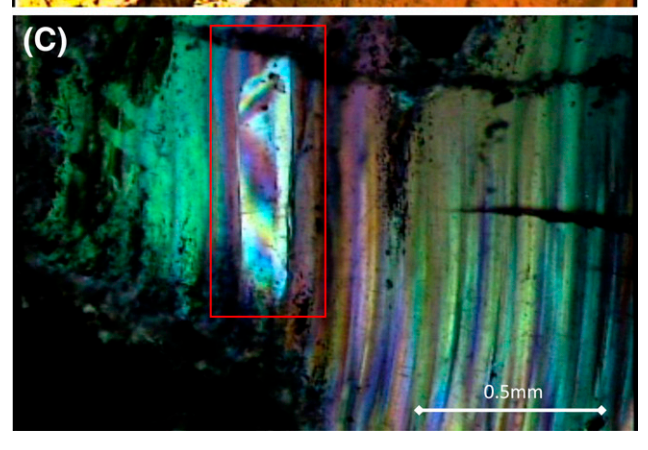


Figure 6. (A, B) Examples of remnant barite (confirmed by scanning electron microscopy/energy-dispersive analysis by x-ray) replaced by fibrous calcite (square). Images in (A) and (B) were used for the guidance of ion microprobe analyses. (C) A cross-polarized transmitted light image of the same area. Birefringence colors are high due to the thickness of the fluid inclusion wafers used for secondary ion mass spectrometry analysis. Pyrite sulfur isotopic compositions in (A) are -21.1% and -17.8% (Vienna Canon Diablo Troilite standard). Barite sulfur isotopic composition in the same bedding-parallel calcite layer in (B) are +22.4% and +21.9%. Note the fibrous calcite beef texture in (C). The samples are from well 9.

penetrated the Haynesville and Bossier shales. These data are summarized in Table A1.5 (supplementary material available as AAPG Datashare 179 at www.aapg.org/datashare) and are shown in Figure 11A–E.

FI Thermometry

The FI homogenization temperatures were measured on selected samples of BPCLs to constrain temperatures of hydrocarbon generation and to elucidate the timing of hydrothermal alteration of the Haynesville and Bossier shales. Figure 12 shows that both aqueous and hydrocarbon inclusions are abundant in BPCLs in the Haynesville shale. It is obvious from Figure 12 that liquid petroleum was present at the time of calcite formation and that this temperature range also transitioned into the timing of early gas generation. In some examples of calcite from BPCLs, the inclusion population is dominated almost exclusively by CH_4 gas, as shown in Figure 13.

Homogenization temperatures for inclusions from wells 1, 2, and 5 used for microlaser Raman spectroscopy are shown in Table A2.1 (supplementary material available as AAPG Datashare 179 at www.aapg.org/datashare). Average primary inclusion temperatures ranged from approximately 145°C to 162°C (Figure A1). We also measured homogenization temperatures in a late-stage subvertical baritecemented chlorite + sphalerite vein from well 2 (Table A2.2 [supplementary material available as AAPG Datashare 179 at www.aapg.org/datashare]). The assemblage of inclusions was the same as seen in Figure 12. The average salinity of the aqueous inclusions based on freezing point depression was approximately 21 wt. % NaCl equivalent. Eutectic melting properties also indicate that the aqueous phase is a CaCl₂- and MgCl₂-rich brine (Tables A2.1, A2.2 [supplementary material available as AAPG Datashare 179 at www.aapg.org/datashare]).

Estimate of In Situ CH₄ Density and Pressure Using Microlaser Raman Spectroscopy

Microlaser Raman spectroscopy was used to measure the in situ density of representative gas-bearing inclusions in thermochemical sulfate reduction (TSR) calcite from BPCLs sampled throughout the

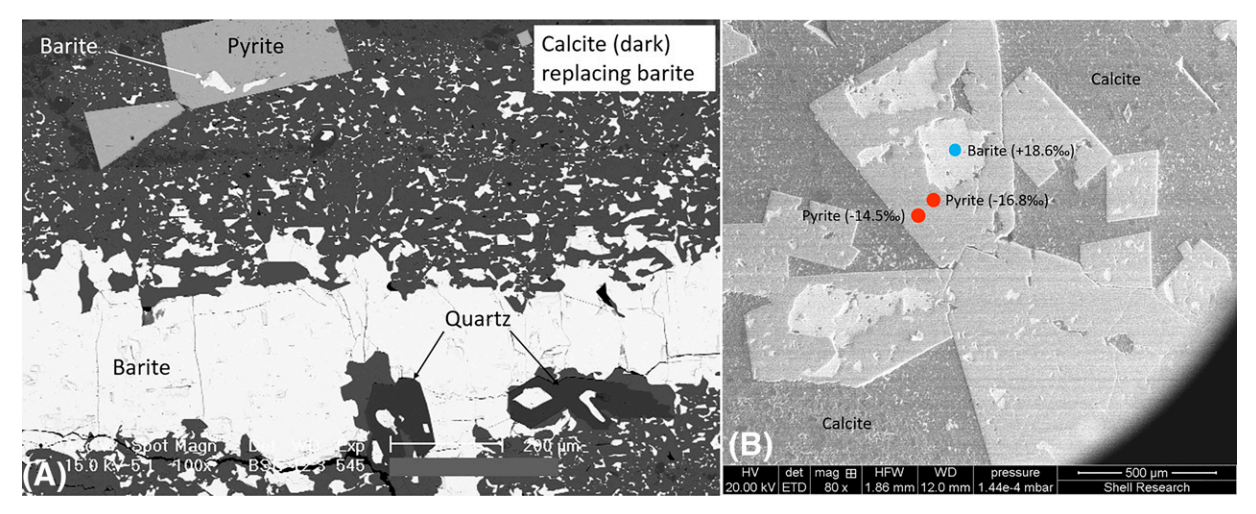


Figure 7. (A) Bedding-parallel calcite layer showing calcite replacement of original bedded barite. (B) Coarse-grained recrystallized euhedral pyrite grains with remnant barite cores. The samples are from well 1. Acc.V = accelerating voltage; BSE = backscattered electron; Det/det = detector; ETD = Everhart Thornley detector; Exp = exposure; HFW = horizontal field width; HV = high voltage; mag/magn = magnification; WD = working distance.

Haynesville shale. The samples analyzed were FI wafers of calcite beef as shown in Figures 5, 6, and 13. Raman spectroscopy is a nondestructive technique that uses a low-energy laser beam to probe a variety of excitations (vibrational modes, in particular) in

molecular moieties in gas, fluid, or solids. The positions of characteristic peaks in Raman spectra for different vibrational modes are referred to as peak shifts.

In the case of CH_4 , it is accepted practice to use the strongest line in the Raman spectrum, which is

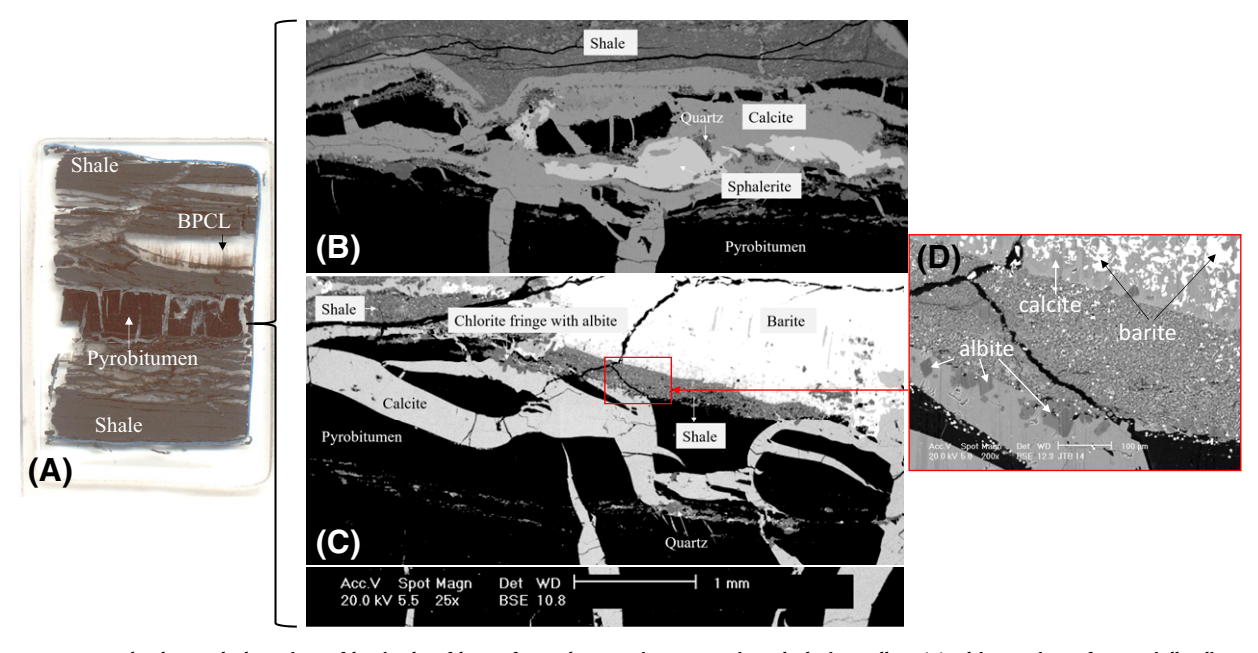


Figure 8. Hydrothermal alteration of barite beef layer from the Bossier Formation shale in well 3. (A) Thin section of a partially disaggregated bedding-parallel pyrobitumen layer adjacent to a bedding-parallel calcite layer (BPCL) with fibrous beef texture. (B) Pyrobitumen layer and late hydrothermal veins containing calcite, quartz, and sphalerite. (C) Hydrothermal veins containing calcite, quartz, chlorite, and albite. (D) Magnification of inset red box in (C), which shows calcite replacement of original bedded barite with a chlorite alteration rim containing euhedral crystals of albite and quartz. Standard thin section in (A) shows context for the bedding-parallel nature of the disaggregated pyrobitumen layer relative to bedding in host shale. The thin section in (A) is 1 in. wide. Acc.V = accelerating voltage; BSE = backscattered electron; Det = detector; Magn = magnification; WD = working distance.

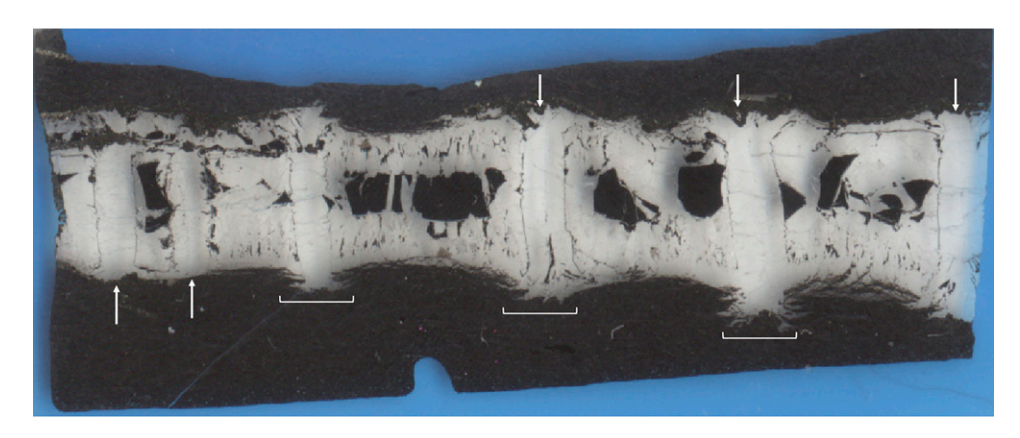


Figure 9. Thin section image of bedding-parallel calcite layer from Haynesville Formation shale well 4. Note the orientation of clean white calcite (arrows) with crystal growth preferentially oriented orthogonally to the original calcite beef fabric. Solid black fragments are pieces of disaggregated pyrobitumen that have been pulled apart due to volume loss associated with replacement of sulfate minerals by calcite, overburden collapse into the original sulfate layer, and growth in the direction of minimum horizontal stress (i.e., parallel to bedding). Calcite splays (brackets) are points of fluid injection from the veins into the shale matrix. Normal 3-in.-wide thin section (7.6 cm). The average bracket length is approximately 0.6 cm.

due to the symmetric CH₄ bond stretching vibration, as referenced in Lu et al. (2007). We have adopted this methodology, along with our own laboratory calibration, for the zero-pressure intercept for the C–H₄ symmetric stretching band in CH₄ (Table A3.1, supplementary material available as AAPG Datashare 179 at www.aapg.org/datashare). Using pressures and sample depths from Table A3.2 (supplementary material available as AAPG Datashare 179 at www.aapg.org/datashare), the average estimated fluid

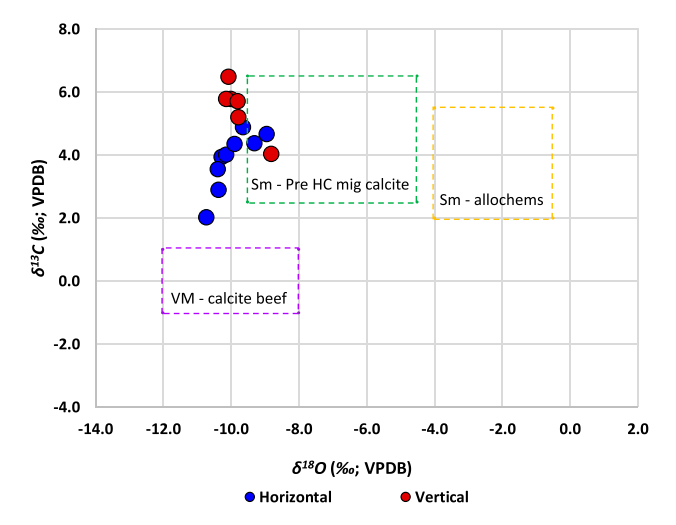


Figure 10. Oxygen and carbon oxygen isotopic composition of calcite from bedding-parallel calcite layers and vertical calcite veins from well 5 (Table A1.1, supplementary material available as AAPG Datashare 179 at www.aapg.org/datashare). HC = hydrocarbon; mig = migration; Sm = Smackover Formation (Heydari and Moore, 1989); VM = Vaca Muerta Formation; VPDB = Vienna Peedee belemnite (Weger et al., 2019).

pressure gradient for our Haynesville wells is approximately 0.87 ± 0.03 psi/ft $(n = 4; \pm 1\sigma)$.

INTERPRETATION AND DISCUSSION

Diagenetic Origin for Beef Textures in BPCLs

Our interpretation of the beef texture in BPCLs is that it represents a primary feature inherited from sedimentary sulfate beds of gypsum and/or barite that were deposited either coevally with or early in the history of the enclosing organic-rich shale. By integrating FI thermometry with oxygen and carbon isotopic data from BPCLs from the Neuquén Basin, we demonstrate that the primary gypsum that was subsequently replaced by anhydrite during burial and compaction of the sediments was also the likely source of water for this diagenetic alteration and replacement process. The transformation of gypsum to anhydrite retains the original primary gypsum texture (Abaab et al., 2021), which has also been described as gypsum beef by Cobbold et al. (2013) or as a stockade-like structure by Roncal-Herrero et al. (2017).

Isotopic Data

The δ^{13} C values for calcite beef layers from the Vaca Muerta Formation reported by Weger et al. (2019) lie in a very tight range of approximately -1% to +1% (VPDB). They are depleted relative to the δ^{13} C

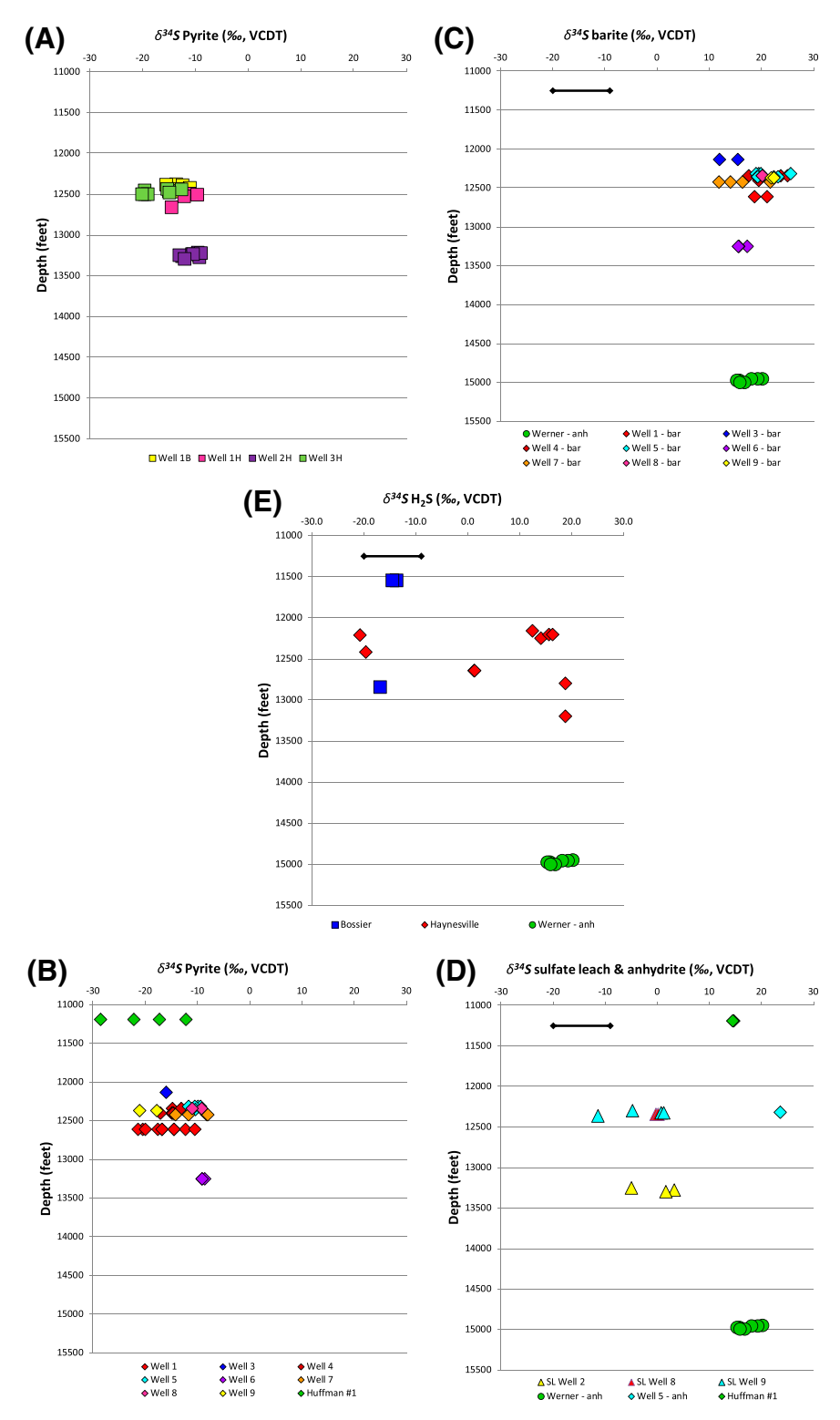


Figure 11. (A) Sulfur isotopic composition of bulk pyrite samples; (B) secondary ion mass spectrometry (SIMS) sulfur isotopic composition of pyrite; (C) SIMS sulfur isotopic composition of barite (bar); (D) sulfate leached from shale matrix samples in wells 2, 3, and 8, and SIMS sulfur isotopic composition of anhydrite (anh); (E) H_2S sampled from various gas wells in the Bossier Formation and Haynesville Formation shales. The solid black bar in (C)–(E) represents the range of $\delta^{34}S$ values for pyrite in (A) and (B). Solid green circles in (C)–(E) are from the underlying Werner anhydrite in the Shell Crocker 1 well. Data are found in Tables A1.2, A1.3, and A1.5, respectively (supplementary material available as AAPG Datashare 179 at www.aapg.org/datashare). SL = sulfate leach; VCDT = Vienna Canon Diablo Troilite standard.

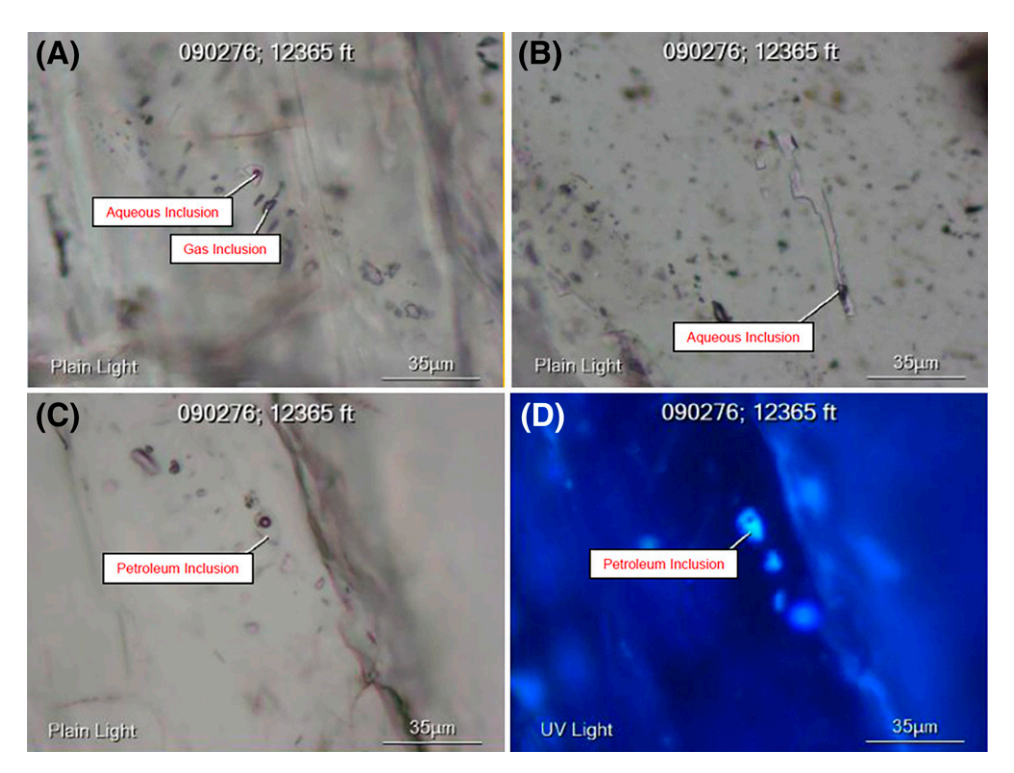


Figure 12. Fluid inclusions in bedding-parallel calcite layers from well 5, showing the presence of aqueous, gas (A, B), and liquid hydrocarbon inclusions (C, D) in calcite. Illumination source as indicated in lower left of each image.

values of calcite beef layers in the Haynesville shale, which range from approximately +2‰ to +5‰ in BPCLs, and approximately +4‰ to +6.5‰ in vertical calcite veins. Weger et al. (2019) reported δ^{18} O of -12% to -9% (VPDB) for calcite in Vaca Muerta beef layers. These values are almost identical to those of the calcite layers in the Haynesville shale, which range from approximately -11% to -9%

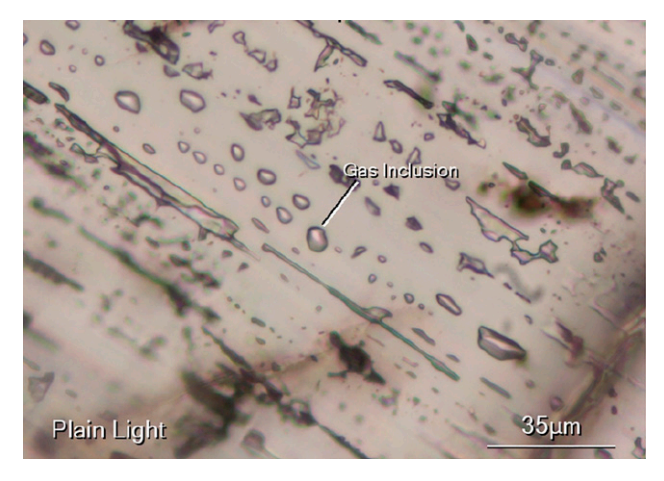


Figure 13. Suite of primary methane gas inclusions trapped along a growth surface in calcite from bedding-parallel calcite layer in Haynesville Formation well 5.

(Figure 10). Weger et al. (2019) attributed the very narrow range of δ^{I3} C values for calcite layers from the Vaca Muerta Formation to buffering by calcite in surrounding mudrocks.

The δ^{I3} C values in Haynesville BPCLs range from +3.5‰ to +6‰ and are almost identical to those in early calcite cements predating hydrocarbon migration in the underlying Smackover Formation, as reported by Heydari and Moore (1989). The similarity of the carbon isotopic compositions of the early calcite cements to those of the Smackover allochems indicated to Heydari and Moore (1989) that the carbon of the calcite was derived and buffered by the host carbonate rock.

Haynesville BPCLs have a more depleted δ^{18} O signature than the Smackover early calcite cements, ranging from -9% to -11% (PDB; Table A1.1 [supplementary material available as AAPG Datashare 179 at www.aapg.org/datashare]). Dissolved and remobilized early calcite cements from either the underlying Smackover Formation or the Haynesville shale itself may explain some of the depleted oxygen isotope data we observe in Haynesville calcite beef layers. Heydari and Moore (1989) observed a similar depletion in δ^{18} O of early calcite in the Smackover

and suggested that the depletion was due to precipitation at progressively higher temperatures during burial. Alternatively, the depleted δ^{18} O signature could indicate precipitation from high-temperature hydrothermal fluids that entered the Haynesville shale at a much later stage, possibly contemporaneously with the timing of the original oil generation and expulsion from the source rock shale.

The Haynesville gas shale has revealed itself to be a very complex system in which H₂S appears to have been generated from multiple sources of sulfur (Figure 11E; Table A1.2 [supplementary material available as AAPG Datashare 179 at www.aapg.org/ datashare]). A proxy for contemporaneous Jurassic seawater sulfate in the study area is provided by the underlying Werner anhydrite (Kampschulte and Strauss, 2004). Both massive and sucrose-textured anhydrite layers are found in the Werner anhydrite. Massive coarsely crystalline Werner anhydrite has a δ^{34} S of +19.2‰ ± 1.1‰ (n = 3; ±1 σ), whereas the fine-grained sucrose-textured samples have a δ^{34} S of $+16.0\% \pm 0.62\%$ (n = 4; $\pm 1\sigma$). Both are consistent with the values of $+18\% \pm 3\%$ for Jurassic seawater from Kampschulte and Strauss (2004) and +17.8% $\pm 0.5\%$ $(n = 10; \pm 1\sigma)$ for Jurassic evaporite sulfur from the Aconcagua-Neuquén Basin of Argentina (Lo Forte et al., 2005). The H₂S sulfur with light $\delta^{34}S = -9\%$ to -20% is most likely derived from original marine kerogen. This isotopically light sulfur is associated with framboidal matrix pyrite having $\delta^{34}S = -11.5\% \pm 2.6\%$ ($n = 22; \pm 1\sigma$). This would be the average sulfur isotopic composition of ubiquitous background levels of H₂S in the Haynesville and Bossier shales. The light and negative H₂S in the Haynesville and Bossier shales is consistent with it being a product of bacterial sulfate reduction (BSR) of contemporaneous marine sulfate, with $\Delta \delta^{34} S_{ox-red}$ of approximately +31% (Machel et al., 1995).

The heavy H_2S sulfur of $\delta^{34}S$ of +16‰ to +18‰ (Figure 11C–E; Table A1.3 [supplementary material available as AAPG Datashare 179 at www.aapg.org/datashare]) is interpreted to be a product of TSR of the original anhydrite and barite layers, with some contribution of aqueous sulfate derived from the dissolution of the underlying Werner anhydrite. The $\delta^{34}S$ of original bedding-parallel barite and anhydrite layers is +19.6‰ \pm 3.6‰ (n = 27; \pm 1 σ). This is indistinguishable from the underlying coarsely crystalline Werner anhydrite (+19.2‰ \pm 1.1‰). It is therefore

not statistically possible to distinguish H_2S produced by TSR of the original bedded sulfate layers that were the likely precursors for most of the BPCLs from TSR of aqueous sulfate derived from dissolution of the underlying Werner anhydrite since both are derived from contemporaneous Jurassic seawater.

Somewhat enigmatic is the apparent sulfur isotopic disequilibrium that exists between original barite and the recrystallized euhedral pyrite that contains remnant barite cores, as shown in Figure 7B. This texture is often considered to be indicative of TSR (Machel et al., 1995), and we would expect the sulfur isotopic composition of the recrystallized pyrite to be the same as that of the barite that it is replacing, but this is not what is observed in Figure 7B. Sulfur isotopic disequilibrium is common between phases containing oxidized and reduced sulfur species and is attributed to slow-reaction kinetics, particularly in hydrothermal systems at temperatures less than approximately 200°C (Ohmoto, 1972).

Sulfate leached from the shale matrix appears to be a mixture of light sulfur from original marine kerogen and framboidal pyrite and a heavy sulfate, typical of the underlying Werner anhydrite. These data suggest that originally there may have been a primary sulfate mineral present in the matrix of the Haynesville shale. Mixing H₂S derived from TSR of the original sulfate, and H₂S derived from the matrix kerogen and framboidal pyrite, produced H₂S with a value of 1.2‰, as shown in Figure 11E. During hydrocarbon generation and expulsion, redox conditions within the organic-rich shale matrix would be highly reducing. Under such conditions, sulfate minerals such as barite and anhydrite are inherently unstable (Worden et al., 1996).

In our study area, we did not observe any remnant sulfate minerals in the matrix of the Haynesville shale. However, researchers at BEG confirmed the presence of abundant primary anhydrite in the matrix of the Haynesville shale in the NFR Energy Huffman 1 gas well in Harrison County, Texas, approximately 60 km to the north-northwest of our study area (J.-P. Nicot, 2012, personal communication; Table A1.5 [supplementary material available as AAPG Datashare 179 at www.aapg.org/datashare]). The sulfur isotopic composition of matrix pyrite in the NFR Energy Huffman 1 well (Figure 11D) is indistinguishable from the sulfur isotopic composition of matrix pyrite shown in Figure 11A and B, respectively.

A puzzling feature of BPCLs that has been documented in organic-rich source rock shales is the notable paucity of barite, relative to celestite, gypsum, and anhydrite (Jewell, 2000; Cobbold et al., 2013). Elmore et al. (2015) documented the common presence of barite often associated with celestite (SrSO₄) in many unconventional shale reservoirs in North America, including the Haynesville shale. In our study, we have not observed celestite associated with BPCLs. We attribute the paucity of barite in organic-rich black shales to its relative instability in the presence of H₂S and hydrocarbons, especially liquid oil, at elevated temperatures and pressure (Machel et al., 1995; Worden et al., 1996; Johnson et al., 2017).

We have documented TSR of both barite and anhydrite in the Haynesville shale and believe that this is the primary reason why so little barite remains in other organic-rich source rocks, particularly in formations that have reached the same degree of thermal maturity experienced by the Haynesville shale. Parts of the Neuquén Basin in Argentina have also experienced episodes of very high heat flow, particularly in areas proximal to Cretaceous volcanism where radiating networks of massive pyrobitumen veins were generated from thermal cracking of organic matter in the organic-rich Vaca Muerta Formation (Cobbold et al., 2013). It is unlikely that much of the primary gypsum beef would be preserved under such conditions, except at the basin margins, where thermal maturity was low and conditions were unfavorable for TSR. In closed-system TSR, with a limited supply of aqueous sulfate, the H₂S will have the same sulfur isotopic composition as its source sulfate. This is exactly what is observed in the Haynesville shale.

Analyses of FIs trapped in BPCLs suggest that early generated liquid hydrocarbons were selectively destroyed through TSR as the result of heating due to an influx of high temperature (approximately 120°C–185°C) and highly saline (approximately 20–25 wt. % equivalent NaCl) Ca- and Mg-rich sulfate brines into the Haynesville shale (Tables A2.1, A2.2 [supplementary material available as AAPG Datashare 179 at www.aapg.org/datashare]). The high salinities, plus the Ca- and Mg-rich nature of the brines are suggestive of an evaporitic source associated with the formation of these sphalerite-bearing barite veins. The most likely source is the underlying Werner anhydrite. This hydrothermal overprint of the Haynesville shale was due to Cretaceous igneous

plutonism that impacted the shales in this part of Louisiana. Hydrothermal fluids remobilized dissolved components from the underlying Werner anhydrite into the overlying Haynesville shale, resulting in TSR and the generation of H_2S with isotopically heavy sulfur. The shallower Bossier shale does not appear to have been impacted by TSR since there is no evidence for evaporite-derived heavy sulfur in H_2S in the Bossier shale (Figure 11E).

Temperature and Timing of BPCLs

Integration of FI thermometry with a calibrated Shell basin model for the Haynesville shale shows that the TSR and contemporaneous hydrothermal activity were associated with Cretaceous (ca. 80-110 Ma) igneous activity that has been well documented in parts of Louisiana, Arkansas, and Mississippi by Morris (1987), Byerly (1991), and Ewing (2009 [his figure 6]). The Sabine island high is associated with the Rusk uplift, radiometrically dated at 90 Ma, whereas ages ranging from 89 to 108 Ma have been reported for igneous rocks associated with the Arkansas igneous province, which are consistent with our own age estimates. This igneous activity is also believed to be responsible for the anomalous presentday high heat flow and overmature nature of the Haynesville source rocks. Pronounced gravity and magnetic anomalies are observed in the Shelby County, Texas, and De Soto Parish, Louisiana, areas underlying the Sabine uplift region (North American Magnetic Anomaly Group, 2002). The anomalies have been modeled as resulting from a mafic igneous mass at depths of 8 to 15 km (Kruger, 2009).

The solid pyrobitumen forming the central parts of most calcite beef layers is a remnant of original liquid oil that was expelled from the source rock and subsequently destroyed by TSR (Novosel et al., 2010). Textural and mineralogical evidence suggests that the locus of TSR was along suture zones at the center of the sulfate-bearing layers, and that this is also the locus of replacement of the original bedded sulfate mineral by TSR-generated calcite beef, as shown in Figures 3 through 8.

Hydrothermal activity documented in the Haynesville shale by Martin and Ewing (2009) and in the present study has many similarities to hydrothermal alteration of organic-rich source rocks in the Posidonia Shale documented by Bernard et al. (2012).

Alteration textures include calcite replacement of barite and anhydrite, chlorite + albite alteration rims, and base metal sulfides such as sphalerite, which are commonly associated with pyrobitumen (Figure 8). Bernard et al. (2012) interpreted these features as indicating alteration of an organic-rich shale by highly saline, high-temperature, hydrothermal fluids during hydrocarbon generation and expulsion, leading to the formation of albite alteration assemblages and pyrobitumen as the degradation product of original liquid oil. We also interpret these features as evidence for a hydrothermal overprint in the Haynesville shale either coeval with or slightly later than the stage of late oil-to-gas generation.

Fluid Sources and Diagenetic Environment

In this section, we examine the oxygen isotopic composition and potential source of water involved in formation of BPCLs. Normally, a value for the oxygen isotopic composition of water is either measured or assumed to permit calculation of the temperature of calcite formation, for example, by using the equilibrium isotope exchange model for calcite-water from Friedman and O'Neil (1977). This method was recently supplemented by the Δ_{47} clumped isotope method of Ghosh et al. (2006) for assessing isotopic equilibrium in the carbonate-CO₂-water system for calcite in BPCLs from Vaca Muerta by Weger et al. (2019).

The Haynesville shale in our study area was deposited in an environment in which gypsum rosettes formed, indicating a shallow water evaporative setting, similar to conditions of evaporite formation in the Neuquén Basin described by Lo Forte et al. (2005) and by Mancini et al. (1990) for Haynesville shale in the Mississippi Interior salt basin of Alabama. De Brodtkorb et al. (1982) and Ramos and de Brodtkorb (1989) proposed an evaporitic origin for the Upper Jurassic-Lower Cretaceous syngenetic celestite and barite deposits in the Neuquén Basin. Digregorio and Uliana (1980) considered these evaporites to be shallow water deposits that transitionally graded into a supratidal sabkha environment. The Mallin Quemado barite ore overlies this gypsum deposit and is up to 10 m thick. Warren (1991, 2006) also recognized an evaporitic origin for thick beds of anhydrite that formed during early burial and dewatering of primary gypsum layers.

Lo Forte et al. (2005) analyzed the oxygen and sulfur isotopes in gypsum from the Neuquén Basin (Table A4.1 [supplementary material available as AAPG Datashare 179 at www.aapg.org/datashare]). For gypsum, they reported δ^{18} O of +13.2‰ ± 1‰ (standard mean ocean water [SMOW]) (n=10; ±1 σ). With this information and the isotopic fractionation factor α^{18} O_{gyp-water} from Liu et al. (2019), it is possible to estimate the oxygen isotopic composition of the water involved in gypsum formation in the Neuquén Basin (see calculation in Table A4.1 [supplementary material available as AAPG Datashare 179 at www.aapg.org/datashare]).

The calculated $\delta^{18}O_{water}$ of approximately +8% (SMOW) is consistent with the lower end of the range reported by Weger et al. (2019) of approximately +8.5% to +14.5% (SMOW). Adopting a value of δ^{18} O for water of approximately +8 \infty and using measured calcite oxygen isotope values of -9%to -11% (VPDB) from Table A1.1 (supplementary material available as AAPG Datashare 179 at www. aapg.org/datashare), we estimate from the watercalcite oxygen isotopic equilibrium of Friedman and O'Neil (1977) a formation temperature range for calcite of approximately 140°C to 165°C (Figure A4.2 [supplementary material available as AAPG Datashare 179 at www.aapg.org/datashare]). We note that these temperatures are in excellent agreement with homogenization temperatures measured on aqueous inclusions shown in Tables A2.1 and A2.2 (supplementary material available as AAPG Datashare 179 at www.aapg.org/datashare). This temperature range is also broadly consistent with that reported by Weger et al. (2019) of 120°C to 150°C in mudrocks and 140°C to 195°C for calcite beef in the Vaca Muerta Formation. We have observed FI homogenization temperatures as high as 186°C to 200°C in some of our Haynesville samples, but these are not typical. A possible explanation for the calcite beef formation temperatures reported by Weger et al. (2019) being elevated relative to the local geothermal gradient could be due to the involvement of TSR. The TSR is an exothermic process (Orr 1974, 1977) and may have reset the Δ_{47} clumped isotope temperatures locally exceeding the regional geothermal gradient, possibly also related to late-stage hydrothermal activity. Otherwise, the reported Δ_{47} clumped isotope temperatures for calcite beef in the Vaca Muerta Formation are in good agreement with our estimated

temperatures for BPCLs in the Haynesville shale. The oxygen isotope data also support a gypsum precursor for the calcite beef layers in the Haynesville shale.

Fluid Pressures during BPCL Formation

One of the features that make the Hayneville shale gas play an attractive asset is the high in situ CH₄ gas pressure, which ensures excellent rates of production. The average fluid pressure gradient for samples in Table A3.2 (supplementary material available as AAPG Datashare 179 at www.aapg.org/datashare) is 0.87 ± 0.03 psi/ft ($\pm 1\sigma$; n = 4), estimated at presentday depth. Gradients would have been even lower in the geological past, before the estimated regional uplift of approximately 1000 to 1500 m. This means that fluid pressures at the time of calcite beef formation were lower than those of the present day and that the calcite beef did not grow under a stress regime in which the fluid pressures ever reached or exceeded overburden pressure. These observations are consistent with those of Wang et al. (2020), who concluded that fibrous BPCLs in Eocene organic-rich shales from Bohai Bay formed under fluid pressures that ranged from approximately 0.5 to 0.6 times lithostatic at temperatures of approximately 125°C to 160°C.

The estimated pressure gradients in Table A3.2 (supplementary material available as AAPG Datashare 179 at www.aapg.org/datashare) are well above hydrostatic but still below the overburden pressure and fracture gradient of the host shale. This has, undoubtedly, contributed to the retention of high CH₄ gas pressures since the time of peak burial when hydrocarbon maturation and subsequent late oil-togas cracking generated most of the CH₄ and pyrobitumen. We agree, therefore, with the observations of Stoneley (1983), Capuano (1994), Rodrigues et al. (2009), Cobbold et al. (2013), and Weger et al. (2019) that there is indeed an obvious connection between the formation of calcite beef, overpressures, and primary oil migration. However, it is the origin of the fibrous calcite beef texture that has not yet been fully appreciated nor recognized in the formation of BPCLs.

Replacement Mechanism by Calcite

In a series of recent experiments that examined the dissolution and growth mechanism during replacement of anhydrite by calcite, Roncal-Herrero et al. (2017) established that calcite growth proceeded by epitactic (epitaxial) nucleation along anhydrite cleavage surfaces and the simultaneous growth of calcite. This process resulted in complete replacement of the anhydrite while preserving the original orientation of the precursor anhydrite. Although no similar experiments were conducted using barite, we note that barite is also an orthorhombic mineral and is isostructural with anhydrite. We expect, therefore, that calcite replacement of barite would proceed in a similar manner (Figures 5, 6).

The replacement of sulfate minerals by calcite is accompanied by a significant negative volume change (Fernandez-Diaz et al., 2009; Roncal-Herrero et al., 2017; Table A5.1 [supplementary material available as AAPG Datashare 179 at www.aapg.org/datashare]). The conversion of gypsum to anhydrite is likely to be a relatively early diagenetic process that occurs in the temperature range of approximately 40°C to 60°C, depending on pore fluid pressure and water activity (i.e., salinity; Jowett et al., 1993), but most likely before any significant hydrocarbon generation. Based on an electron backscatter diffraction study on calcite crystal habit and forms in fibrous calcite layers from Bohai Bay, Ma et al. (2020) showed that the calcite crystals had sharp rhombohedral shapes and hexagonal prism morphology. According to Li (1994), these types of calcite crystal forms indicate low temperatures of formation, approximately 25°C to 75°C.

The replacement reactions of relevance to the Haynesville BPCLs are therefore the conversion of barite and anhydrite to calcite, associated with estimated volume losses of approximately 29 and approximately 20 vol. %, respectively (Table A5.1 [supplementary material available as AAPG Datashare 179 at www.aapg.org/datashare]). For the case of the anhydrite replacement by calcite, Roncal-Herrero et al. (2017) noted that some of this negative volume of reaction forms interstitial porosity in the anhydrite-gypsum network. However, only some of this volume loss can be accommodated as porosity.

We infer that median sutures in calcite beef layers represent breaks in the accumulation and episodic evaporation of sulfate-saturated brines and are horizons defined by accumulation of clay and silt particles. As zones of structural weakness, they represent permeable pathways that allowed for the

migration and expulsion of $CO_2 \pm$ brine \pm hydrocarbons out of the organic-rich source rock shale. Replacement of sulfate occurred from this median suture outward toward the layer margins, as shown in Figures 3D, 5A–F, and 6C, in which incomplete replacement of barite by calcite is observed. A volume loss of approximately 20% to 30% during replacement by calcite also creates space into which the remaining assemblage of solids and fluid must be redistributed. This provides a plausible explanation for the brittle deformation textures that characterize the distribution of disaggregated solid pyrobitumen at the centers of calcite beef layers, as shown in Figures 3D, 8A, and 9.

Where the replacement of sulfate minerals by calcite is more pronounced and the volume loss is greatest, calcite continues to nucleate and grow. However, in these cases, due to the collapse of the BPCL, the preferred growth orientation of the calcite is in the direction of minimum stress-in other words, orthogonal to the original calcite beef texture. An example of this is shown in Figure 9. The mechanism by which the solid pyrobitumen was disaggregated is due to a combination of compression by the overburden stress σ_{ν} , extension in the direction of minimum horizontal stress, and shrinkage of pyrobitumen volume from oil-to-gas cracking. This resulted in stretching and tensile failure of the brittle pyrobitumen into adjacent void space created by volume loss during the replacement of barite and anhydrite by calcite. Late-stage calcite growth associated with this late phase of compaction also resulted in fluid loss out of the BPCL into the shale matrix. Figure 9 clearly shows such fluid expulsion features as splays of calcite forcibly disrupting bedding at the contacts with adjacent shale matrix. We interpret these splay features as points where fluids were forcibly injected into the shale matrix. Similar calcite textures have been reported in the middle Tuscaloosa Formation mudstone and in the Havnesville shale by Lu et al. (2011) and by Hammes and Frébourg (2012; Figure 10F), respectively.

In their study of calcite beef in the Vaca Muerta Formation, Rodrigues et al. (2009) also observed a second generation of pyrobitumen-free white calcite that appeared as an outer zone in which the calcite crystals were deformed, forming an oblique angle between the original vertical fibrous calcite and the wall rock shale. They attributed the deformation to

horizontal stresses due to tectonic shortening, which probably postdated peak gas generation in the Vaca Muerta Formation. The Vaca Muerta Formation experienced horizontal shortening during BPCL formation (Rodrigues et al., 2009; Ukar et al., 2017). By contrast, the Haynesville shale is bounded by the North Louisiana Salt Basin to the east and the East Texas Salt Basin to the west (Figure 1). Any horizontal tectonic stress would likely be ameliorated by salt movement before any significant horizontal shortening impacted the Haynesville shale. Even so, we have also observed horizontal offsets bounded by median sutures in the Haynesville shale shown in Figure 3A, B, for example.

CONCLUSION

Our mineralogical, isotope geochemistry, FI, and Raman spectroscopic studies provide new data that bear directly on how BPCLs formed. Mineralogical precursors to these layers are shown to be dominated by syngenetic layers of early, low-temperature sulfate minerals, principally gypsum and barite. Our work shows that the fibrous calcite beef texture of BPCLs is an inherited feature attributable to the replacement of early sulfate minerals, deposited in evaporite-rich basins by authigenic calcite.

In the Haynesville shale, H2S was generated from two well-defined sources of sulfur. Isotopically light H₂S sulfur with $\delta^{34}S = -9\%$ to -20% is most likely derived from original marine kerogen and is associated with framboidal matrix pyrite, with $\delta^{34}S =$ $-11.5\% \pm 2.6\%$ (*n* = 22; $\pm 1\sigma$), consistent with the formation by BSR of contemporaneous marine sulfate. Heavy H₂S has $\delta^{34}S = +16\%$ to + 18\% and formed by TSR. Sulfur derived from the reaction of bedding-parallel barite and anhydrite layers (δ^{34} S = +19.6% $\pm 3.6\%$; n = 27; $\pm 1\sigma$) is indistinguishable from the underlying Werner anhydrite. We conclude that the heavy H2S was produced by TSR of sulfate minerals precipitated from Jurassic seawater and remobilized aqueous sulfate from the Werner anhydrite introduced into the Haynesville shale by later hydrothermal activity associated with Cretaceous plutonism.

Using recently published fractionation factors for oxygen isotopes in the gypsum-water system (corrected for salinity), we estimate the oxygen isotopic composition of water involved in the deposition of primary gypsum to be approximately +8‰ (SMOW). Together with the measured oxygen isotope values of -9% to -11% (PDB) in calcite, we estimate from the water-calcite oxygen isotopic equilibrium of Friedman and O'Neil (1977) a formation temperature range for calcite of approximately 140° C to 165° C. This range of temperatures is in excellent agreement with FI homogenization temperatures measured in fibrous calcite and late hydrothermal barite veins.

The oxygen isotope data are also consistent with gypsum dehydration being a significant source of water associated with the diagenetic replacement of primary gypsum by authigenic calcite in BPCLs in both the Haynesville shale and the Vaca Muerta Formation.

Results of microlaser Raman spectroscopy show that CH₄ pressures associated with the replacement of sulfate by TSR and the formation of the BPCLs were likely well below the overburden stress and did not exceed the local fracture gradient. This ensured retention of high saturations and pressures of CH₄ gas generated by secondary oil-to-gas cracking. Oil-to-gas cracking also generated the pyrobitumen layers that typically are observed along the median sutures in BPCLs.

The replacement of anhydrite and barite by calcite is associated with a significant negative volume of reaction of approximately 20 to 30 vol. %. A consequence of such a volume loss of solid material is the collapse of the original sulfate beef layer and redistribution of solid pyrobitumen through disaggregation in the direction of minimum horizontal stress. At maximum volume loss and under compression by the overburden stress, newly formed calcite grew orthogonally to the original calcite beef fabric, also in the direction of minimum horizontal stress (i.e., parallel to bedding).

REFERENCES CITED

- Abaab, N., A. Zanella, D. Akrout, R. Mourgues, and M. Montacer, 2021, Timing and distribution of bedding-parallel veins, in evaporitic rocks, Bouhedma Formation, Northern Chotts, Tunisia: Journal of Structural Geology, v. 153, 104461, 17 p., doi:10.1016/j.jsg.2021.104461.
- Bernard, S., B. Horsfield, H.-M. Schulz, R. Wirth, A. Schreiber, and N. Sherwood, 2012, Geochemical evolution of organic-rich shales with increasing maturity: A STXM and TEM study of the Posidonia Shale (Lower Toarcian,

- northern Germany): Marine and Petroleum Geology, v. 31, no. 1, p. 70–89, doi:10.1016/j.marpetgeo.2011.05.010.
- Bryndzia, L. T., and N. R. Braunsdorf, 2014, From source rock to reservoir: The evolution of self-sourced unconventional resource plays: Elements, v. 10, no. 4, p. 271–276, doi:10.2113/gselements.10.4.271.
- Bryndzia, L. T., and C. I. Macaulay, 2018, H₂S in Unconventional Resource Plays: Occurrence, origin, and mechanisms of formation: 1st European Association of Geoscientists and Engineers/French Institute of Petroleum Conference on Sulfur Risk Management in Exploration and Production, Rueil-Malmaison, France, September 18–20, 2018, doi:10.3997/2214-4609.201802763.
- Bryndzia, L. T., C. Macaulay, and A. Litvinchuk, 2017, Understanding controls on EUR in the Haynesville shale gas play: It's all about the in situ density and pressure of methane gas (abs.): AAPG Annual Convention and Exhibition, Houston, Texas, April 2–5, 2017, accessed November 1, 2023, http://www.searchanddiscovery.com/abstracts/html/2017/90291ace/abstracts/2611982.html.
- Byerly, G. R., 1991, Igneous activity, *in* A. Salvador, ed., The Gulf of Mexico Basin: The geology of North America, Boulder, Colorado, Geological Society of America, p. 91–108, doi:10.1130/DNAG-GNA-J.91.
- Capuano, R. M., 1994, Evidence of fluid flow in microfractures in geopressured shales: Reply: AAPG Bulletin, v. 78, no. 10, p. 1641–1646, doi:10.1306/A25FF247-171B-11D7-8645000102C1865D.
- Cobbold, P. R., A. Zanella, N. Rodrigues, and H. Løseth, 2013, Bedding-parallel fibrous veins (beef and cone-incone): Worldwide occurrence and possible significance in terms of fluid overpressure, hydrocarbon generation and mineralization: Marine and Petroleum Geology, v. 43, p. 1–20, doi:10.1016/j.marpetgeo.2013.01.010.
- Cody, R. D., and A. M. Cody, 1988, Gypsum nucleation and crystal morphology in analog saline terrestrial environments: Journal of Sedimentary Petrology, v. 58, no. 2, p. 247–255, doi:10.1306/212F8D69-2B24-11D7-8648 000102C1865D.
- de Brodtkorb, M. K., V. Ramos, M. Barbieri, and S. Ametrano, 1982, The evaporitic celestite-barite deposits of Neuquen, Argentina: Mineralium Deposita, v. 17, no. 3, p. 423–436, doi:10.1007/BF00204470.
- Digregorio, J. H., and A. Uliana, 1980, Cuenca Neuquina, *in* J. C. Turner, ed., Geologia regional Argentina: Academia Nacional de Ciencias, Cordoba, Argentina II, p. 985–1032.
- Eberli, G. P., R. J. Weger, M. Tenaglia, L. Rueda, L. Rodriguez, M. Zeller, D. F. McNeill, S. Murray, and P. K. Swart, 2017, The unconventional play in the Neuquén Basin, Argentina Insights from the outcrop for the subsurface: Society of Petroleum Engineers/AAPG/Society of Exploration Geophysicists Unconventional Resources Technology Conference (URTeC), Austin, Texas, July 24–26, 2017, URTeC: 2687581, 12 p., doi:10.15530/URTEC-2017-2687581.
- Elmore, R.D., Dulin, S.A., Manning, E.B., Steullet, A.K., Benton, A, Dennie, D., Roberts, J., Heij, G., and Deng, J., 2015, Paragenesis of mineralized fractures in organic rich shales: AAPG Search and Discovery article 51178, accessed

- November 5, 2018, https://www.searchanddiscovery.com/pdfz/documents/2015/51178elmore/ndx_elmore.pdf.html.
- Eustice, R. A., and L. S. Land, 1994, Controls on the deposition of bedded halite in the Haynesville Formation, Champion-Klepac No. 1 core, southwestern Alabama: Gulf Coast Association of Geological Societies Transactions, v. 44, p. 217–224.
- Ewing, T. E., 2009, The ups and downs of the Sabine Uplift and the northern Gulf of Mexico Basin: Jurassic basement blocks, Cretaceous thermal uplifts, and Cenozoic flexure: Gulf Coast Association of Geological Societies Transactions, v. 59, p. 253–269.
- Fernandez-Diaz, L., C.C. Pina, J.M. Astilleros, and N. Sanchez-Pastor, 2009, The carbonation of gypsum: Pathways and pseudomorph formation: American Mineralogist, v. 94, p. 1223–1234, doi:10.2138/am.2009.3194.
- Friedman, I., and J. R. O'Neil, 1977, Compilation of stable isotope fractionation factors of geochemical interest: Washington, DC, US Geological Survey Professional Paper 440-KK, 117 p., doi:10.3133/pp440KK.
- Gale, J. F. W., S. E. Laubach, J. E. Olson, P. Eichhubl, and A. Fall, 2014, Natural fractures in shale: A review and new observations: AAPG Bulletin, v. 98, no. 11, p. 2165–2216, doi:10.1306/08121413151.
- Ghosh, P., J. Adkins, H. Affek, B. Balta, W. Guo, E. A. Schauble, D. P. Schrag, and J. M. Eiler, 2006, ¹³C–¹⁸O bonds in carbonate minerals: A new kind of paleothermometer: Geochimica et Cosmochimica Acta, v. 70, no. 6, p. 1439–1456, doi:10.1016/j.gca.2005.11.014.
- Hammes, U., and G. Frébourg, 2012, Haynesville and Bossier mudrocks: A facies and sequence stratigraphic investigation, East Texas and Louisiana, USA: Marine and Petroleum Geology, v. 31, no. 1, p. 8–26, doi:10.1016/j.marpetgeo.2011.10.001.
- Hammes, U., Hamlin, H. S., and Ewing, T. E., 2011, Geologic analysis of the Upper Jurassic Haynesville Shale in east Texas and west Louisiana: AAPG Bulletin, v. 95, no. 10, p. 1643–1666, doi:10.1306/02141110128.
- Heydari, E., and C. M. Moore, 1989, Burial diagenesis and thermochemical sulfate reduction, Smackover Formation, south eastern Mississippi salt basin: Geology, v. 17, no. 12, p. 1080–1084, doi:10.1130/0091-7613(1989)0 17<1080:BDATSR>2.3.CO;2.
- Hilgers, C., and J. L. Urai, 2005, On the arrangement of solid inclusions in fibrous veins and the role of the crack-seal mechanism: Journal of Structural Geology, v. 27, no. 3, p. 481–494, doi:10.1016/j.jsg.2004.10.012.
- Jewell, P. W., 2000, Bedded barite in the geological record, in C. R. Glenn, L. Prevot-Lucas, and J. Lucas, eds., Marine authigenesis: From global to microbial: Tulsa, Oklahoma, SEPM Special Publication 66, p. 147–161, doi:10.2110/ pec.00.66.0147.
- Johnson, C. A., N. M. Piatak, and M. M. Miller, 2017, Barite (barium), in K. J. Schulz, J. H. DeYoung Jr., R. R. Seal II, and D. C. Bradley, eds., Critical mineral resources of the United States—Economic and environmental geology and prospects for future supply: Washington, DC, US Geological Survey Professional Paper 1802-D, 30 p., doi: 10.3133/pp1802D.

- Jowett, E.C., Cathles, L.M., Davis, B.W., 1993, Predicting depths of gypsum dehydration in evaporitic sedimentary basins: AAPG Bulletin, v. 77, p. 402–413, doi:10.1306/BDFF8C22-1718-11D7-8645000102C1865D.
- Kampschulte, A., and Strauss, H., 2004, The sulfur isotopic evolution of phanerozoic seawater based on the analysis of structurally substituted sulfate in carbonates: Chemical Geology, v. 204, p. 255–286, doi:10.1016/j.chemgeo. 2003.11.013.
- Kruger, J. M., 2009, Regional gravity anomalies of the Ouachita orogenic belt, southern Oklahoma aulacogen, and adjacent Gulf Coastal Plain: Implications for the tectonic evolution of the south-central U.S.: Geological Society of America Abstracts with Programs, v. 41, no. 2, p. 27–28.
- Lejay, A., S. Larmier, P. Rutman, and F. Gelin, 2017, The Role of porosity in the development of Parallel bedded calcite filled fractures (or beef) in the Vaca Muerta: An integrated analysis from high resolution core data: Society of Petroleum Engineers/AAPG/ Society of Exploration Geophysicists Unconventional Resources Technology Conference (URTeC), Austin, Texas, July 24–26, 2017, URTeC: 2668071, 16 p., doi:10.15530/urtec-2017-2668071.
- Li, R., 1994, Characters of forms and surface microstructure of calcite crystals occurred in polymetallic deposits in south Hunan: Hunan Geology, v. 13, no. 1, p. 25–28.
- Liu, T., E. Artacho, F. Gazquez, G. Walters, and D. Hodell, 2019, Prediction of equilibrium isotopic fractionation of the gypsum/bassanite/water system using first-principles calculations: Geochimica et Cosmochimica Acta, v. 244, p. 1–11, doi:10.1016/j.gca.2018.08.045.
- Lo Forte, G. L., F. Orti, and L. Rosell, 2005, Isotopic characterization of Jurassic evaporites. Aconcagua-Neuquén Basin, Argentina: Geologica Acta, v. 3, no. 2, p. 155–161.
- Lu, J., K. Milliken, R. M. Reed, and S. Hovorka, 2011, Diagenesis and sealing capacity of the middle Tuscaloosa mudstone at the Cranfield carbon dioxide injection site, Mississippi, U.S.A.: Environmental Geoscience, v. 18, no. 1, p. 35–53, doi:10.1306/eg.09091010015.
- Lu, W., I.-M. Chou, R. C. Burrus, and Y. Song, 2007, A unified equation for calculating methane vapor pressures in the CH₄–H₂O system with measured Raman shifts: Geochimica et Cosmochimica Acta, v. 71, no. 16, p. 3969–3978, doi:10.1016/j.gca.2007.06.004.
- Ma, C., C. Dong, D. Elsworth, Q. Wang, Z. Huang, H. Liu, G. Luan, et al., 2020, Insights from electron backscatter diffraction into the origins of fibrous calcite veins in organic-rich shale from lower Es3 to upper Es4, Jiyang Depression, China: Marine and Petroleum Geology, v. 113, 104131, 11 p., doi:10.1016/j.marpetgeo.2019. 104131.
- Machel, H. G., 1985, Fibrous gypsum and fibrous anhydrite in veins: Sedimentology, v. 32, no. 3, p. 443–454, doi:10. 1111/j.1365-3091.1985.tb00523.x.
- Machel, H. G., H. R. Krouse, and R. Sassen, 1995, Products and distinguishing criteria of bacterial and thermochemical sulfate reduction: Applied Geochemistry, v. 10, no. 4, p. 373–389, doi:10.1016/0883-2927(95)00008-8.

399

- Małachowska, A., S. Green, and J. Hupka, 2017, Properties and formation of mineralized veins in an organic-rich shale formation: 51st US Rock Mechanics/Geomechanics Symposium, San Francisco, California, June 25–28, 2017, ARMA-201700635.
- Mancini, E. A., B. H. Tew, and R. M. Mink, 1990, Jurassic sequence stratigraphy in the Mississippi interior salt basin of Alabama: Gulf Coast Association of Geological Societies and Gulf Coast Section of SEPM meeting, Lafayette, Louisiana, October 17–19, 1990, p. 521–529.
- Martin, B. J., and T. E. Ewing, 2009, Ancestral basin architecture—A possible key to the Jurassic Haynesville trend, *in* T. Carr, T. D'Agostino, W. Ambrose, J. Pashin, and N. C. Rosen, eds., Unconventional energy resources: Making the unconventional conventional, Tulsa, Oklahoma, SEPM, p. 511–515, doi:10.5724/gcs.09.29.0203.
- Morris, E. M., 1987, The Cretaceous Arkansas alkalic province: A summary of petrology and geochemistry, *in* E. M. Morris and J. D. Pasteris, eds., Mantle metasomatism and alkaline magmatism: Geological Society of America Special Paper 215, p. 217–234, doi:10.1130/SPE215-p217.
- North American Magnetic Anomaly Group, 2002, Magnetic anomaly map of North America: US Geological Survey Special Map, scale 1:10,000,000.
- Novosel, I., K. Manzano-Kareah, and A. S. Kornacki, 2010, Characterization of source rocks in the Greater Sabine Bossier and Haynesville Formations, northern Louisiana USA (abs.): AAPG Annual Conference and Exhibition, New Orleans, Louisiana, April 11–14, 2010, accessed November 1, 2023, https://www.searchanddiscovery.com/pdfz/abstracts/pdf/2010/annual/abstracts/ndx_novosel.pdf.
- Ohmoto, H., 1972, Systematics of sulfur and carbon isotopes in hydrothermal ore deposits: Economic Geology, v. 67, no. 5, p. 551–578, doi:10.2113/gsecongeo.67.5.551.
- Orr, W. L., 1974, Changes in sulfur content and isotopic ratios of sulfur during petroleum maturation Study of Big Horn Basin Paleozoic oils: AAPG Bulletin, v. 58, p. 2295–2318, doi:10.1306/83D91B9B-16C7-11D7-8645000102C1865D.
- Orr, W. L., 1977, Geologic and geochemical controls on the distribution of hydrogen sulfide in natural gas, in R. Campos and J. Goni, eds., Advances in organic geochemistry: Madrid, Spain, Enadimsa, p. 571–597.
- Ramos, V. A., and M. K. de Brodtkorb, 1989, Celestite, barite, magnesite, and fluorspar: Stratabound settings through time and space, *in* M. K. de Brodtkorb, ed., Nonmetalliferous stratabound ore fields: New York, Van Nostrand Reinhold, p. 297–321.
- Rodrigues, N., P. R. Cobbold, H. Løseth, and G. Ruffet, 2009, Widespread bedding parallel veins of fibrous calcite ("beef") in a mature source rock (Vaca Muerta Fm, Neuquén Basin, Argentina): Evidence for overpressure and horizontal compression: Journal of the Geological

- Society, v. 166, no. 4, p. 695–709, doi:10.1144/0016-76492008-111.
- Roncal-Herrero, T., J. M. Astilleros, P. Bots, J. D. Rodríguez-Blanco, M. Prieto, L. G. Benning, and L. Fernández-Díaz, 2017, Reaction pathways and textural aspects of the replacement of anhydrite by calcite at 25°C: American Mineralogist, v. 102, no. 6, p. 1270–1278, doi:10. 2138/am-2017-5963CCBY.
- Stoneley, R., 1983, Fibrous calcite veins, overpressures, and primary oil migration: Geologic note: AAPG Bulletin, v. 67, p. 1427–1428, doi:10.1306/03B5BA47-16D1-11D7-8645000102C1865D.
- Ukar, E., R. G. Lopez, J. F. Gale, S. E. Laubach, and R. Manceda, 2017, New type of kinematic indicator in bed-parallel veins, Late Jurassic–Early Cretaceous Vaca Muerta Formation, Argentina: EW shortening during Late Cretaceous vein opening.: Journal of Structural Geology, v. 104, p. 31–47, doi:10.1016/j.jsg.2017.09.014.
- van der Pluijm, B., and S. Marshak, 2004, Joints and veins, in Earth structure: An introduction to structural geology and tectonics, 2nd ed.: New York, W. W. Norton, p. 138–165.
- Wang, M., Y. Chen, W. M. Bain, G. Song, K. Liu, Z. Zhou, and M. Steele-MacInnis, 2020, Direct evidence for fluid overpressure during hydrocarbon generation and expulsion from organic-rich shales: Geology, v. 48, no. 4, p. 374–378, doi:10.1130/G46650.1.
- Warren, J. K., 1991, Sulfate-dominated sea-marginal and platform evaporative settings: Sabkhas and Salinas, mudflats and salterns: Developments in Sedimentology, v. 50, p. 69–187, doi:10.1016/S0070-4571(08)70260-7.
- Warren, J. K., 2006, Evaporites: Sediments, resources and hydrocarbons: New York, Springer, 1035 p., doi:10. 1007/3-540-32344-9.
- Weger, R. J., S. T. Murray, D. F. McNeill, P. K. Swart, G. P. Eberli, R. L. Blanco, M. Tenaglia, and L. E. Rueda, 2019, Paleothermometry and distribution of calcite beef in the Vaca Muerta Formation, Neuquen Basin, Argentina: AAPG Bulletin, v. 103, no. 4, p. 931–950, doi:10.1306/10021817384.
- Wiltschko, D. V., and J. W. Morse, 2001, Crystallization pressure versus "crack seal" as the mechanism for banded veins: Geology, v. 29, no. 1, p. 79–82, doi:10.1130/0091-7613(2001)029<0079:CPVCSA>2.0.CO;2.
- Worden, R. H., P. C. Smalley, and N. H. Oxtoby, 1996, The effects of thermochemical sulfate reduction upon formation water salinity and oxygen isotopes in carbonate gas reservoirs: Geochimica et Cosmochimica Acta, v. 60, no. 20, p. 3925–3931, doi:10.1016/0016-7037(96)00216-5.
- Zanella, A., P. R. Cobbold, and T. Boassen, 2015, Natural hydraulic fractures in the Wessex Basin, SW England: Widespread distribution, composition, and history: Marine and Petroleum Geology, v. 68, p. 438–448, doi:10.1016/j.marpetgeo.2015.09.005.